PO Box 2345, Beijing 100023, China
www.wjgnet.com
wjg@wjgnet.com

World J Gastroenterol 2007 January 14; 13(2): 192-218
World Journal of Gastroenterology ISSN 1007-9327

TOPIC HIGHLIGHT

Parimal Chowdhury, Professor, *Series Editors*

Advances in small animal mesentery models for *in vivo* flow cytometry, dynamic microscopy, and drug screening

Ekaterina I Galanzha, Valery V Tuchin, Vladimir P Zharov

Ekaterina I Galanzha, Vladimir P Zharov, Philips Classic Laser Laboratories, University of Arkansas for Medical Sciences (UAMS), Little Rock, AR, United States
Ekaterina I Galanzha, Valery V Tuchin, Department of Optics and Biomedical Physics, Research-Educational Institute of Optics and Biophotonics, Saratov State University, Saratov, Russia
Supported by NIH/NIBIB; No. EB001858, EB-000873, EB005123
Correspondence to: Ekaterina I Galanzha, MD, PhD, DSc, Philips Classic Laser Laboratories, University of Arkansas for Medical Sciences (UAMS), 4301 W. Markham St., Little Rock, AR 72205-7199, United States. egalanzha@uams.edu
Telephone: +1-501-5267620 Fax: +1-501-6868029
Received: 2006-10-10 Accepted: 2006-11-30

Key words: Lymph microcirculation; Transmission digital microscopy; Rat mesentery; Flow cytometry; Photothermal technique

Galanzha EI, Tuchin VV, Zharov VP. Advances in small animal mesentery models for *in vivo* flow cytometry, dynamic microscopy, and drug screening. *World J Gastroenterol* 2007; 13(2): 192-218

http://www.wjgnet.com/1007-9327/13/192.asp

Abstract

Using animal mesentery with intravital optical microscopy is a well-established experimental model for studying blood and lymph microcirculation *in vivo*. Recent advances in cell biology and optical techniques provide the basis for extending this model for new applications, which should generate significantly improved experimental data. This review summarizes the achievements in this specific area, including *in vivo* label-free blood and lymph photothermal flow cytometry, super-sensitive fluorescence image cytometry, light scattering and speckle flow cytometry, microvessel dynamic microscopy, infrared (IR) angiography, and high-speed imaging of individual cells in fast flow. The capabilities of these techniques, using the rat mesentery model, were demonstrated in various studies; e.g., real-time quantitative detection of circulating and migrating individual blood and cancer cells, studies on vascular dynamics with a focus on lymphatics under normal conditions and under different interventions (e.g. lasers, drugs, nicotine), assessment of lymphatic disturbances from experimental lymphedema, monitoring cell traffic between blood and lymph systems, and high-speed imaging of cell transient deformability in flow. In particular, the obtained results demonstrated that individual cell transportation in living organisms depends on cell type (e.g., normal blood or leukemic cells), the cell's functional state (e.g., live, apoptotic, or necrotic), and the functional status of the organism. Possible future applications, including *in vivo* early diagnosis and prevention of disease, monitoring immune response and apoptosis, chemo- and radio-sensitivity tests, and drug screening, are also discussed.

INTRODUCTION

It is difficult to access the gastrointestinal tract with powerful intravital high-resolution optical microscopy. One unique exception is the mesentery, which has as its main functions maintaining digestive organs in their proper positions while simultaneously providing routes for nerves and for blood and lymph vessels. To date, small animal mesentery is a well-established experimental model for studying blood and lymph microcirculation *in vivo*.

Historically, the first microscopic observation of the mesenteric lymph microvessels of a guinea pig was performed by Arnold Heller in 1869[1]. During the first 30-50 years of the 20th century, extensive *in vivo* studies of mesenteric microcirculation were undertaken[2-4]. In particular, the basics of capillary circulation were first studied in rat mesentery[3]. Later, this model was successfully used to study the fundamentals of the microvascular physiology of blood (i.e., microvascular rheology, hemodynamics, vasomotion, hematocrit, permeability of the vascular wall, flow velocity) and lymph (i.e., phasic contractile activity, flow velocity, and the diameter of small lymphatics) systems[5-26]. Using rat mesentery, Sekizuka *et al*[24] performed real-time videoanalysis of contractile lymphatic motion in rat mesentery and determined quantitatively the dynamics of the frequency of these contractions. Benoit *et al*[22] and Dixon *et al*[26] obtained basic data about relationships among lymphatic contractile activity, vessel diameter, and lymph flow velocity[23]. In particular, they established the correlation between cyclic fluctuations of lymph velocity

and vessel wall motion during the phasic contraction. Most of the results related to microvessel diameter and contractile activity were obtained with conventional transmission optical microscopy alone.

The mesentery model has also been used to study the effects of various hormones, mediators, drugs, and other environmental impacts on microcirculation, including the influence of histamine, norepinephrine, dopamine, dobutamine, PO_2, substance P, L-NAME, methylene blue, leukotrienes, histamine, platelet activating factor, temperature, low-power laser radiation, X-radiation, and others[3,20,27-34]. In particular, this model was used in the first study of the effects of nitric oxide (NO) on lymph microvessels *in vivo*: Shirasawa *et al*[35] showed the influence of a NO synthase inhibitor on lymphatic diameter and contractile activity, which was reversed after applying an endogenous NO donor (L-arginine). This model has also been employed to study microcirculation disturbances in experimental models of diseases such as diabetes, ischemia, hemorrhage, shock, inflammation, tumor, edema, and others[2,4,13,21,22,36,37].

Recent discoveries in cell biology (e.g., identification of the genes, such as VEGF-C and VEGF-D, expressed by endothelium or endothelial growth factors for lymphatics), along with advances in optical techniques (e.g., lasers, high-speed digital cameras, powerful software) have increased interest in this model and its capabilities for studying the fundamentals of blood and lymph microcirculation, including its potential for the molecular imaging of individual cells *in vivo*[38-40]. Nevertheless, some methods used in most experiments have limitations. For example, the majority of the results about platelets [e.g., platelet thrombosis, or their interaction with white blood cells (WBCs) or vessel walls], red blood cells (RBCs), and tumor cells were obtained with what are currently the most powerful techniques, such as fluorescent labe ling[12,13,21,41-43]. However, despite significant progress in the development of new labels[44-46] (e.g., quantum dots, fluorescent-specific antibodies[47]), these techniques *in vivo* (as in many other experiments *in vitro*) are potentially subject to photobleaching (despite the short exposure time), or cytotoxicity. Moreover, growing evidence shows that fluorescence labeling may seriously distort genuine cell properties, even without evident toxicity, and cellular physiologic functions. For example, acridine orange and Rhodamine 6G, traditional fluorescent dyes for leukocytes, have been demonstrated to be mutagenic and carcinogenic, and possibly cause phototoxic effects[48-51]. Fluorescence imaging of lymphatics by injecting fluorescein isothiocyanate (FITC)-dextran into the interstitial space led to elevated interstitial pressure and altered lymph viscosity[52]. These findings may raise some concern about the kinetics of labeled cells in flow, particularly about the main cause and the real rate of cell elimination from circulation, the actual properties of apoptotic or cancer cells, or the strong influence of the tags due to phagocytosis, or the interaction of tags with other cells[53-55]. All these concerns gain importance in *in vivo* studies in humans, and add to interest in developing label-free imaging. The mesentery model with advanced optical technique can provide a good quality of label-free imaging of moving cells.

In mesenteric microvessels, the imaging of flowing cells *in vivo* without any staining or labeling was realized mainly with transmission microscopy for slow moving, rolling (30-70 μm/s), and adhesive WBCs[10,12,14,15,17]. The monitoring of single RBCs and their small aggregates has usually been performed in two modes: 1) in selected microvessels (small venules or capillaries) with slow flow using a frame rate of 20-30 frames per second (fps), or 2) using a short time-exposure mode (~0.1-1 ms) by which only single images of fast-moving cells can be captured[56-58]. Only a few studies demonstrated relatively high-speed imaging for measuring flow velocity in the range of 750-2500 fps in blood flow, and approximately 500 fps in lymph flow[19,26,59]. Due to motion distortion, these speeds are not quite fast enough to image shape and subcellular structures of individual fast-moving cells. For example, imaging in blood microvessels, with typical flow velocities of 5-10 mm/s, requires imaging speed ranges of 5000-10 000 fps[58]. Additionally, simultaneous high-speed imaging with high optical resolution of individual moving cells has not yet been developed *in vivo*. This is crucial for *in vivo* flow cytometry (FC).

In this review, which is based on our 15 years of experience in this area, we summarize both our previous data, which are scattered or presented in difficult-to-access publications, as well as our latest achievements in *in vivo* label-free FC, high-speed imaging, and vessel dynamics, focusing on real-time monitoring of circulating and migrating blood and cancer cells in blood and lymph systems, and especially on our studies of microlymphatic function in normal and pathological states and under the impact of different therapeutic interventions.

FEATURES OF THE LYMPHATIC SYSTEM

Unlike the circular blood network, the lymphatic vasculature is an open-ended system that transports lymph from tissue to the blood system[60,61]. The initial lymphatics collect fluid and cells from the interstitial space of tissue and form the afferent (prenodal) lymph, which is transported through valvular prenodal lymphatics to the lymph nodes. In the lymph nodes, some fluid, debris, and pathogens are removed from lymph, while cells (mainly lymphocytes) are added to lymph. Lymph leaves the lymph node by efferent collecting lymphatics, and passes through the thoracic duct and enters into the inferior vena cava. During this process, some cells and proteins can re-circulate in the blood system-tissue-lymph system-blood system pathway. In contrast to blood, which is moved by one motor, the heart, the motion of lymph is primarily maintained by rhythmic contractions of vessel walls, called phasic contractions. Such contractions are initiated by pacemakers along vessels. Additionally, lymph vessels have well-developed bicuspid funnel-shaped valves (collagen sheets with filaments covered on both sides by endothelium), which are dispersed at regular intervals along the vessel and divide it into functional units-lymphangions (the fragment of the lymph vessel between input and output valves). The valves can block lymphatic lumen to prevent (at least partially) backflow and contribute to a

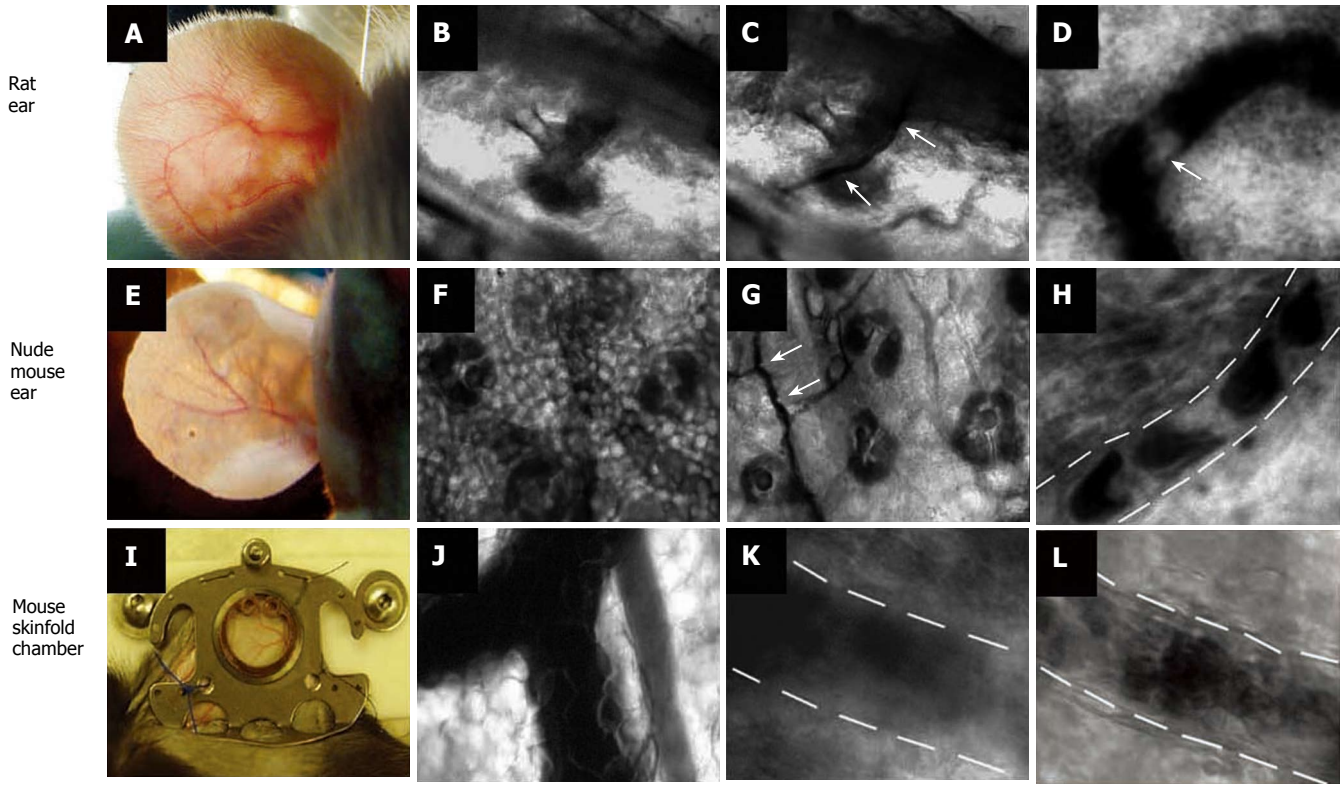

Figure 1 Label-free imaging of blood vessels in different animal models. Rat ear (with hair): **A**: External view of large vessel; **B**, **C**: transmission images of microvessel at low magnification (4 ×) before (**B**) and after (**C**) topical administration of an optical clearing agent such as glycerol (arrows show microvessel); **D**: high-resolution image of rolling WBC (arrow) in a venula (magnification 40 ×). Ear of nude mouse: **E**: external view of large vessels; **F**, **G**: transmission images of microvessels at low magnification (10 ×) before (**F**) and after (**G**) topical administration of glycerol (arrows show microvessel); **H**: high-resolution image of individual RBCs in a capillary (magnification 100 ×); **I**: large vessels in skinfold chamber of a mouse; **J**: transmission image of blood microvessel at low magnification (10 ×); **K**, **I**: high-resolution image of a venula before (**K**) and after (**I**) topical administration of glycerol (40 ×).

unidirectional flow. Some external forces, such as muscle contractions, respiratory movements, and intestinal peristalsis, can also maintain lymph motion. In general, lymph flow is turbulent, has an oscillating character, and is slower than blood motion. The lymphatics in an entire living organism have multi-level regulation, including the central nervous system, hormones, and local substances such as mediators, pH, and Ca ions[1,24,26,29,60-69].

Compared to the well-studied blood system, our understanding of lymph function is limited; however, rat mesentery, with its unique structure that we describe here, may help to fill knowledge gaps in this under-explored system. Below, we present a brief comparison of different animal models emphasizing the advantage of rat mesentery for monitoring single-cell transport under normal and pathologic conditions.

ANIMAL MODELS

Microcirculation has been successfully studied using optical microscopy in various animal models (e.g., rabbit or mouse ear, hamster or mouse dorsal skin-flap window or skin-fold chamber, or open cremaster muscle)[52-55,59,63,70-73]. The use of these models for high-resolution imaging of individual flowing or static cells may be somewhat limited because of significant light scattering from surrounding tissue (e.g., skin or muscles) and/or the relatively deep location of vessels below the skin. Image quality in these particular models can be improved in two ways: (1) by using thin hairless skin (e.g. ear of nude mouse ~270 μm thick), or (2) by decreasing light scattering using a recently developed optical clearing method combined with spectral selection (e.g. use a "green" filter to increase blood vessel contrast)[74-77].

Figure 1 illustrates our few attempts using these models and transmission microscopy to obtain high-resolution images of individual cells in blood flow without staining. In particular, we compared images of blood microvessels of ordinary (i.e. with hair, Figure 1A-D) and nude (i.e., hairless, Figure 1E-H) ear skin of rats and mice, and with mouse dorsal skin-fold chamber (Figure 1I-L). The best results were obtained with the nude mouse ear model in combination with optical clearing and a spectral filter in the range of the maximum absorption of hemoglobin, around 570-580 nm (Figure 1F-H). The dorsal skin-fold model provided a poorer quality image of an individual cell as compared with the RBC images of the skin-fold chamber (Figure 1L) and with RBC images of nude mouse ear (Figure 1H), and required an invasive procedure. In general, even after many improvements, all of these models provide monitoring of individual cells only in selected capillaries with single-file flow (RBCs travel in one line with the same velocity). In addition, the images of colorless lymphatics in skin can be obtained mainly with additional labeling with fluorescent or absorbing contrast agents (e.g. FITC-dextran and dyes such as isosulfan blue,

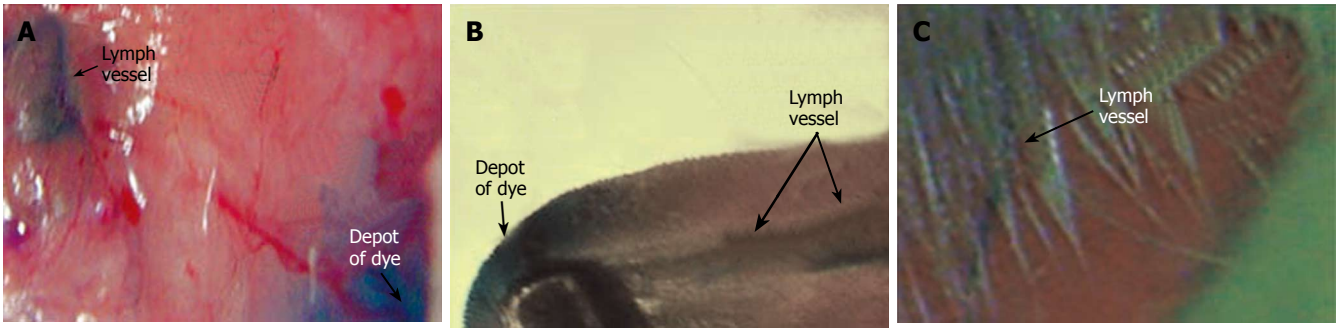

Figure 2 Imaging of lymph vessels using contrast agents in different rat models. Lymphatics labeled by a 1% solution of lymphazurin in muscles of (**A**) abdomen wall, (**B**) tongue, and (**C**) pad.

lymphazurin, and others; Figure 2)[52,78-80]. However, these procedures do not provide information on cell dynamics in flow or valve functioning.

In general, the best targets for conventional transmission microscopy are relatively transparent animal structures such as zebrafish, and vascular nets of the hamster cheek pouch[63,81-84]; however, these models are not ideal for studying lymph or blood vessels. The zebrafish (tropical fish) model is very different from human anatomy and physiology, and while the hamster cheek pouch model is good for visualizing blood microvessels, the lymphatics in the hamster cheek pouch are not well developed, preventing us from simultaneously studying blood and lymph systems, if desired.

To date, the best optical images of both lymph and blood microvessels have been obtained in the mesentery of small cold-blooded (frog) and mammalian (mouse, cat, rabbit, guinea pig, and rat) animals. However, the capillaries of frog mesenteric microvessels are relatively larger in diameter and their sensitivity to environmental impacts is markedly less than that of mammals[3]. Of the mammalian models, the rat is an excellent model in terms of size, physiology, and pharmacokinetics for broadening medical applications, including single-cell diagnostics[85-88]. Additionally, some rat models are able to mimic select human diseases. This is particularly important for understanding common mechanisms of microvessel physiology and pathology (edema, inflammation, tumor), as well as for studying specific features of mesenteric microvasculature under normal conditions (to maintain homeostasis in the abdominal space) and in mesentery-related diseases (e.g. mesothelioma, sclerosing mesenteritis, panniculitis, acute mesenteric vein thrombosis, tumor metastasis).

Mesentery consists of thin (8-15 μm), relatively transparent, duplex connective tissue, which is divided into triangular, relatively transparent windows by arteries (400-500 μm in diameter) and veins (600-700 μm in diameter) obscured by adipose tissue (Figure 3D)[3,89-91]. The smaller branches of these vessels leave the adipose regions and pass into the microvascular net (Figure 3E), which spreads out into transparent areas. On the venous side of the capillaries, there is an accumulation of initial lymphatics (Figure 3E-G). These initial lymphatics then pass into larger valvular lymphatics, which are located parallel with and very close to the venules (Figure 3E, H).

Thus, rat mesentery triangulars contains all the typical components of a microvascular net: a blood microvessel network including arterioles (diameter, 7-60 μm; velocity, 5-10 mm/s), venules (10-70 μm; 0.5-3 mm/s), and capillaries (5-9 μm; 0.1-1.4 mm/s), as well as well-developed microlymphatic vessels (diameter, 50-250 μm; velocity 0-7 mm/s) and clearly distinguishable initial lymphatics with migrating cells[3,24,26,58,66,92-94]. Figure 3 shows typical images obtained with the optical schematics portrayed in Figure 4.

The specific functional features of mesenteric vasculature involve a considerable gradient of venular permeability, a preponderance of fluid filtration, and a relatively low proportion (~15%) of re-absorption of interstitial fluid by capillaries[95,96]. Additionally, rat mesenteric blood microvascular is characterized by many communications between the capillary loops arising from neighboring arterioles with well-developed arterio-venous anastomoses, which shunt blood from arteriola to venula[3]. This structure can facilitate adaptation and maintenance of blood flow under different conditions.

For medical imaging, the main advantage of mesenteric microcirculation is that a single layer of blood and well-developed lymph microvessels lies in one plane (Figure 4B), which facilitates continuous observation of all components of the microvascular network (from arteriola to venula, together with lymph microvessels, Figure 3H), as well as label-free, high-resolution imaging of individual cells with almost ideal optical conditions (Figure 3I-N). Light is slightly attenuated, mainly in the relatively thin vessel wall, without any influence from other tissues, as it is in other models. The refractive indexes in the typical spectral range of 400-700 nm used for studies are lower for rat mesenteric tissue (n = 1.38) than for rat skin (n = 1.40-1.42) and, especially, for the epidermis (n = 1.55) for humans; thus, it is close to that of water (n = 1.33)[97]. As a result, these optical and geometric features significantly reduce unwanted scattered light, allowing the use of a microscopic objective with a high numerical aperture (up to 1.4) and high magnification (60× - 100×). Optical reflectance spectra from lymph vessels obtained *in vivo* with a fiber optic spectrometer (Model 1000, Ocean Optics, Inc., USA) demonstrated slight spectral features and time-dependence within 1-2 s (Figure 5), which can

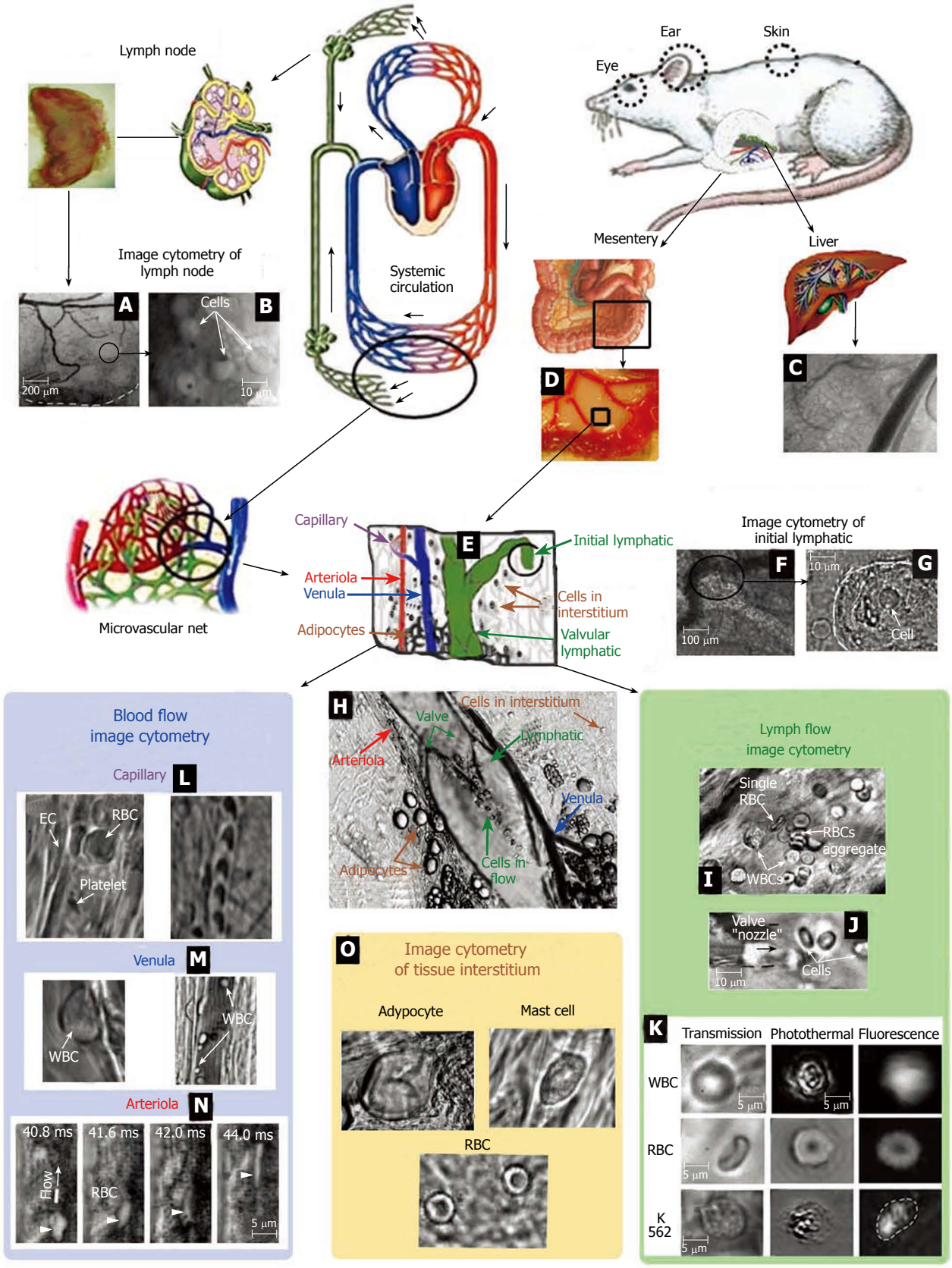

Figure 3 *In vivo* monitoring of microcirculation using rat mesentery. **A**, **B**: Sections of a single lymph node at different magnifications (4 × and 100 ×, respectively); **C**: liver section (10 ×); **D**: section of intestine with mesentery; **E**: schematic of typical tissue microvascular unit; **F**, **G**: initial lymphatic (4 × and 100 ×); **H**: section of mesenteric tissue with valvular lymph vessel and surrounding blood vessels (10 ×); **I**: high-resolution imaging of single WBCs and RBCs, as well as their aggregates in lymph flow (100 ×); **J**: valve tip with fast-flowing cells (100 ×); **K**: transmission, photothermal, and fluorescence images of individual WBC, RBC, and K562 leukemic cell in lymph flow; **L**: capillary at different magnifications, (left) high-resolution images of RBCs, platelets, and endothelial cells (EC) in capillary wall (100 ×) and (right) parachute-like RBCs at low magnification (10 ×); **M**: rolling WBC in venula (100 ×, 10 ×); **N**: four sequential high-resolution images of RBC shapes in fast arteriolar flow (velocity of 5 mm/s; 40 ×); **O**: high-resolution images of adipocyte, mast cell, and RBCs in the interstitial space (100 ×).

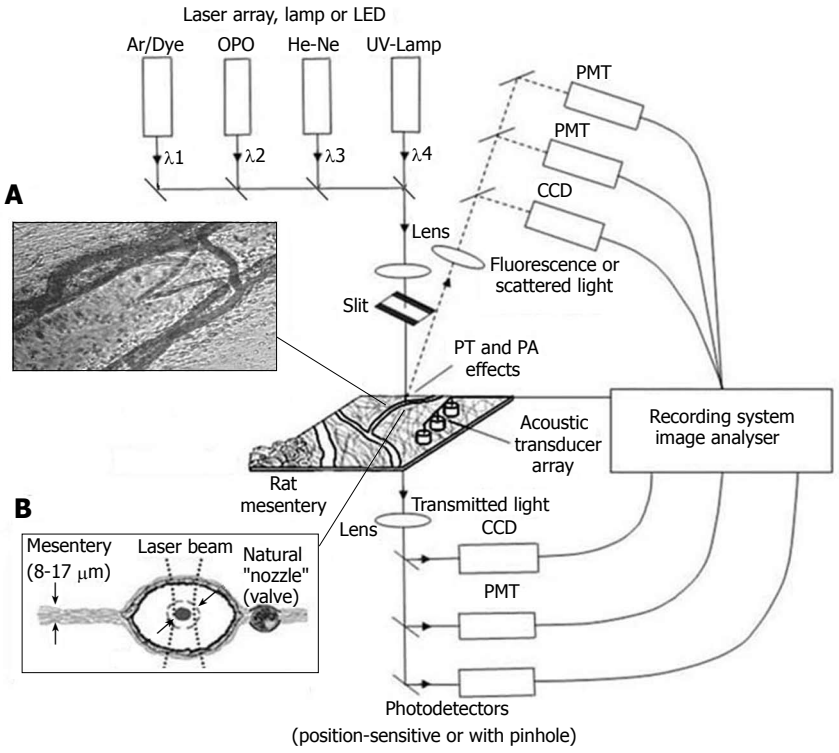

Figure 4 Integrated, multispectral FC *in vivo*. **A**: Typical transmission image of rat mesentery segment with lymph and blood microvessels; **B**: Schematic of the mesentery cross-section.

be explained by specific lymph flow oscillations[98]. An additional advantage of the mesenteric model is the good penetration of the reagents into the mesenteric lining. Thus, the responses of the microvascular network to different environmental impacts can be studied relatively easily using a simple topical application.

The well-developed procedure for preparing rat mesentery for studying microcirculation include anesthetizing the rat (ketamine/xylazine, 50/10 mg/kg, i.m.), followed by a laparotomy by mid-abdominal incision (~1 cm), gently exteriorizing the intestinal loop with mesentery from the abdomen and positioning it on a customized thermostabilizing microscope stage, which maintains the body temperature at approximately 37.7℃ [2,3,22-28,35,58,66,94]. The mesentery is bathed with a constant diffusion of warm Ringer's solution with a phosphate buffer and 1% bovine serum albumin (37℃, pH 7.4). In principle, these procedures may introduce some limitations and artifacts related to the anesthesia, the minimal but invasive surgical intervention, and periodic small vibrations of the mesentery due to intestinal motion[19,99]. However, according to experimental data gathered during at least 2-3 h of acute observation after microsurgery, these procedures do not produce marked changes in microvessel function (diameter, phasic activity, valve function, lymph flow) or in metabolic or respiratory parameters. Furthermore, the short timeframe during which the rapidly circulating cells are in the microvessels of the exposed mesenteric area significantly reduces the influence of this exposure on the properties of the flowing cells. Additionally, to decrease the effects of the surgical manipulations and to stabilize the microvascular parameters, the monitoring of cells in blood and lymph flow begins approximately 15 min after the laparotomy[93]. Coating the intestinal loop with oxygen-impermeable plastic foil helps maintain stable physiological

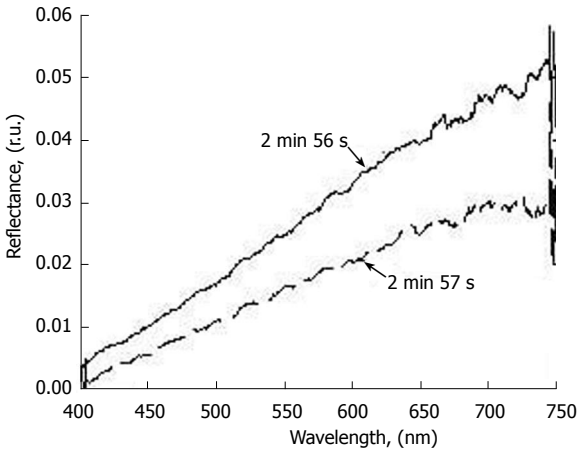

Figure 5 Time-resolved reflection spectra from the same point on the lymphatic vessel (D = 128 μm) at different times.

parameters for up to 5 h[100]. Our data also demonstrate that it is possible to repeat the surgical procedure to periodically monitor the same microcirculation area during the development of chronic pathology, even over a 2-mo timeframe[101]. To exclude the influence of microsurgery itself on the microcirculation, the data from experimental groups were usually compared with those from the corresponding control group, which undergo a mid-abdominal microincision without any other interventions.

In general, based upon our experience and the experiences of other groups, this easy-to-access mesentery microvessel model, which has significant features and advantages (see above) with only a few minor limitations, is a very promising vehicle for real-time monitoring, with the highest optical resolution, of individual static, migrating, and circulating cells (e.g. WBCs, RBCs, cancer cells, and

many others). Such a model is essential for studying immune function and the transport of proteins, cells, and liquid between the blood and lymph systems under normal and pathologic (lymphedema, metastasis, and many other lymph-related diseases) states.

INTEGRATED IMAGING SYSTEM

Recent progress in optical techniques enabled the development of a multi-module, multi-functional experimental system that integrates transmission digital microscopy (TDM), a photothermal (PT) method, a highly sensitive fluorescent and speckle technique with advanced charge-coupled device (CCD) or complementary metal oxide semiconductor (CMOS) cameras (Figure 4). The primary application of this system was for *in vivo* FC. Indeed, although *in vitro* FC is a powerful, established diagnostic method[102], only an *in vivo* study can assess physiologic and pathologic processes involving cell metabolism and cell-cell interactions (e.g., adhesion, aggregation, rolling effects, migration through vessel walls) in the real, complex environment of living organisms[53-55,84,99,103]. Further, invasive isolation of cells from their native environment and their processing may not only introduce artifacts, but also make it impossible to examine the same cell population over long time periods. Adaptation of FC for *in vivo* studies required overcoming problems related to light scattering by vessel walls and surrounding tissues, fluctuation of cell velocity, cell position in a vessel, and precautions with labeling procedures[53,54].

TDM module

TDM was built on the technical platform of an upright Olympus BX-51 microscope and provides the following functions: (1) imaging of relatively large structures such as lymph and blood microvessels with relatively low magnification (4 × -10 ×, Figure 3H); (2) quantitative dynamic evaluation of blood and lymph microvessel diameter, parameters of lymphatic phasic contractions and valve activity, and cell concentration in flow; (3) determination of cell velocity in lymph flow by video-recording cell movement [so-called particle image velocimetry (PIV)];[18,19] (4) navigation of the pulse laser beams on the desired area of the mesentery in other optical methods; and (5) single-cell identification at high magnification (40 ×, 60 ×, and 100 ×, water immersion)[58,94,104]. In particular, the mesentery model provides a unique opportunity to simultaneously image *in vivo*, with the highest optical resolution (~300 nm), individual cells in blood microvessels (Figure 3L and M) and small lymphatics (Figure 3F, G, I-K), tissue interstitium (Figure 3O), and lymph nodes (Figure 3A and B) located in the root of the mesentery and even in the liver.

The images were recorded with several digital cameras: a black-and-white Cohu 2122 and a color Nicon DXM1200, with speeds up to 25 fps and a minimal exposure time of 0.04 s. These speeds were sufficient to image relatively slow-moving individual cells, such as rolling leukocytes (30-70 μm/s), in blood flow (Figure 3M). We also used a highly sensitive CCD camera (Cascade 650, Photometrics) with speed of up to 500 fps and with a minimal exposure time of 0.1 ms. A high-speed CMOS camera (model MV-D1024-160-CL8; Photonfocus, Switzerland), with speeds of 10 000 fps for an area of 128 × 128 pixels and 39 000 fps for an area of 128 × 16 pixels, provided high-resolution imaging of fast-moving RBCs in blood flow (2-10 mm/s in arterioles and large venules, Figure 3N) and WBCs in valvular lymphatics (ranging from 0 to 7 mm/s). Scion Image (Scion Corp.), Nicon software (ACT-1), and WinX/32 V2.5.18.1 (Roper Scientific) were used for processing, capturing, measuring, and editing images of the moving cells.

Using TDM in the bright-field mode, the combination of light absorption and scattering effects on cells made it possible to visualize and identify most blood cells without conventional labeling and vital staining. In particular, due to relatively strong light absorption by RBCs, these single cells in flow appeared mostly as dark objects in the trans-illumination mode, while weakly absorbing WBCs and platelets appeared either as light objects (e.g., in the presence of many more strongly absorbing RBCs in blood flow or with dominant scattering effects) or, in contrast, as slightly dark objects (e.g., in the transparent plasma without RBCs). In the "packed" flow, RBCs sometimes exhibited bright margins or were seen as light objects due to multiple scattering effects. This is because the light, during propagation through many other RBCs and before reaching the plane of focus, was significantly scattered and attenuated through absorption, resulting in dominant scattering light around imaged cells.

The integration of high-resolution and high-speed monitoring improves PIV in the dynamic range and enhances spatial resolution and measurement accuracy. In particular, our technique enables us to measure the velocity of individual cells up to 10 mm/s without marked optical distortion of cell images in packed multi-file blood flow[104]. However, the low absorption sensitivity of TDM makes it impossible to differentiate individual cells with slight differences in absorption in fast flow *in vivo* (e.g. different WBCs or cancer cells).

PT module

To detect low-absorbing cells, PT methods were used with no cell labeling and inherence to scattered light. With these methods, absorption by non-fluorescent cellular components (most of which are naturally weakly fluorescent) is measured by monitoring thermal (due to picosecond-scale non-radiative relaxation of the absorbed energy) and accompanying effects directly in cells[105-109]. For non-fluorescent samples, PT methods currently offer the highest sensitivity for the absorption coefficient, on the order of 10^{-5}-10^{-6} cm^{-1}, which makes it possible to non-invasively (a short-term temperature elevation ⩽ 1-5℃) detect a single, unlabeled biomolecule with a sensitivity comparable to that of laser-fluorescence methods (i.e. with labeling)[109-111]. This absorption sensitivity threshold of the PT technique is at least four to five orders of magnitude better (e.g., 10^{-2}-10^{-3} cm^{-1} for single cells) than that of TDM, with the capability to measure absorption spectra at the subcellular level in weakly absorbing cells (e.g. WBCs

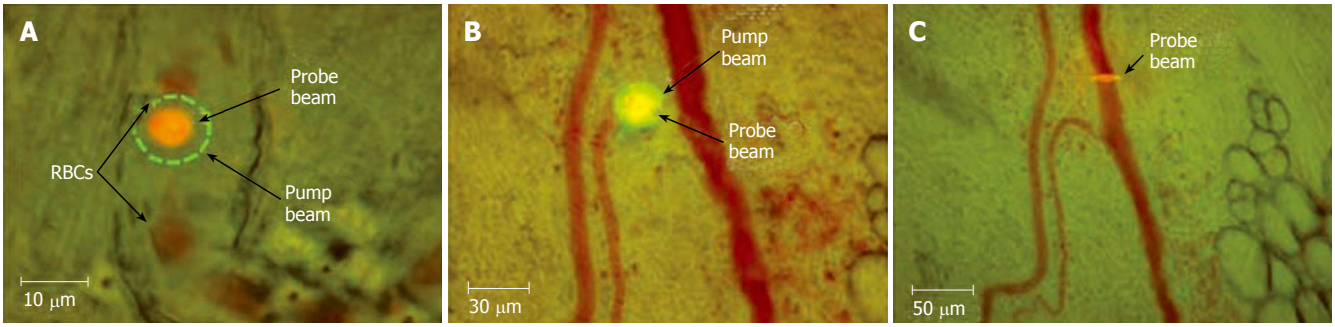

Figure 6 Typical positions of probe (red) and pump (green) laser beams during PT imaging. **A**: Circular beams in a blood capillary (cell velocity, ~0.5 mm/s; magnification, 100 ×); **B**: Overlapping pump and probe pulses in an artery (cell velocity, ~2 mm/s; magnification, 10 ×); **C**: an ellipsoidal beam geometry in a blood vessel (cell velocity, ~5 mm/s; magnification, 10 ×).

or cancer cells).

Briefly, in the first PT imaging (PTI) mode, individual cells were irradiated with a short, focused pump laser pulse of a tunable optical parametric oscillator (OPO) laser (wavelength, 420-2300 nm; pulse width, 8 ns; pulse energy, 0.1-10^3 μJ; Lotis Ltd., Minsk, Belarus; Figure 6)[109,112,113]. Time-resolved monitoring of temperature-dependent variations of the refractive index around the absorbing cellular structures or whole cells was accomplished with thermal-lens (thermolens) or phase-contrast imaging (Olympus BX51 microscope with a CCD camera; AE-260E, Apogee Inc.) using a second, collinear laser pulse of a Raman shifter (wavelength, 639 nm; pulse width, 13 ns; pulse energy, 10 nJ). In particular, in the phase contrast mode, a customized phase-contrast microobjective (20 ×) with a Zernike coaxial quarter-wave filter was used to image the probe laser beam. The diameters of the pump- and probe-beam spots were varied 20-40 μm and 15-25 μm, respectively.

A second thermolens mode made it possible to record a whole cell's time-resolved integral PT response *via* the defocusing effects of a collinear, intensity-stabilized He-Ne laser probe beam (wavelength, 633 nm; diameter, 15 μm; energy, 2 mW) as detected with a photodiode through a pinhole (0.5 mm). The PT response was recorded with a Tektronix TDS 3032B oscilloscope. In the presence of gaps between neighboring cells in lymph and blood flow (typical for small lymphatics and blood capillaries), we used a circular laser-beam geometry (Figure 6A). At short distances, selected experiments were performed with an elliptical beam shape (Figure 6C).

In contrast to TDM, the PT technique was able to identify low-absorbing cells (e.g. normal and apoptotic WBCs or cancer cells) in blood and lymph flow *in vivo* on the basis of their differences in integral and local absorption associated with specific heme proteins[58,77,94,114-118].

Laser speckle microscopy (LSM) module

Because of the varying velocities and trajectories of cell motion in cross-sections of vessels, time-consuming TDM is not well suited for rapidly estimating mean cell velocity in the presense of many cells in flow. The limitations of TDM were partially solved using the LSM technique (Figure 7)[66,68,98,119-122]. Laser radiation from a focused He-Ne laser beam (633 nm) scattered by a diffusely scattering object has a specific, speckle structure (Figure 7A and B), resulting from the interference of independent contributions from a large number of randomly distributed scattering centers. Detection of the speckle fluctuation' s intensity (Figure 7C) with a photodetector provides information of flow velocity estimated through the width of the power spectrum of these fluctuations or from the width of their autocorrelation function (Figure 7D and E). Figure 7D illustrates the spectrum recorded for the central part of a vessel (axial lymph flow), while Figure 7E demonstrates spectra obtained at points placed near the vessel wall. Such changes indicate that velocity decreases from a vessel's center to its periphery, which enables monitoring of the profile patterns of lymph-flow velocity for microlymphatics.

To increase its ability to measure the absolute value and direction of flow, we also used the speckle-correlation mode, which uses two photodetectors to record the intensity in fluctuations of the speckle field at two points[123,124]. The described algorithm was verified *in vivo* by measuring lymph flow in a lymphatic vessel with LSM (Figure 7F curve 1) and TDM (Figure 7F curve 2). There was relatively good correlation (coefficient of linear regression = 0.72) between the two methods; however, the LSM mode had advantages, such as rapid calculation of lymph-flow velocity (compared to TDM). On the other hand, combining LSM with TDM allowed us to: (1) monitor the quantitative dynamics of cell velocity in lymph or blood flow; (2) verify data from the speckle method; (3) obtain a profile of lymph velocity through the changing shapes of the speckle signal from the center region to the near-wall region; and (4) determine the dynamic relationships among changes in lymph flow velocity and other functional activities of lymphatics. This integrated schematic also has the potential for speckle-imaging of mesenteric structures at cellular and subcellular levels, including detection of individual cell rotation and functional state (e.g., live, apoptotic, and necrotic) in flow[118].

Fluorescent module

A fluorescence module was added to the integrated system to verify PT data and for independent applications using specific fluorescent tags to identify different cells with similar shapes and sizes (e.g. lymphocytes and leukemia

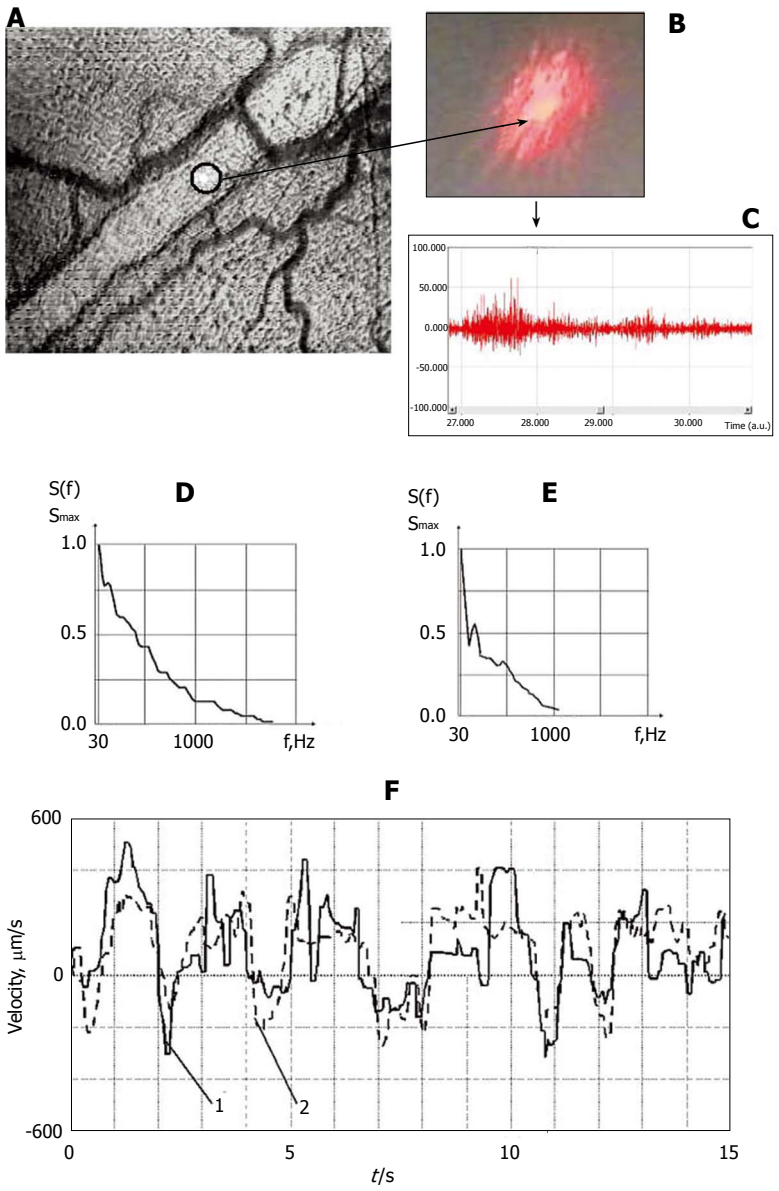

Figure 7 Integration of laser speckle and transmission microscopies for studying lymph flow dynamics. **A**: A laser beam was focused into a small-diameter spot (~5 μm) on axial lymph flow (microvessel diameter 55 μm); **B**: Lymph flow randomly modulated the focused Gaussian beam to provide scattered dynamic speckles images; **C**: Scattered intensity fluctuations were detected by a photodetector and transformed into an electrical output signal. **D** and **E**: Spectral shapes from scanning the lymphatic cross-section: (**D**) the spectrum when the laser beam was focused in axial flow and (**E**) when the laser beam was focused in flow near the lymphatic wall; **F**: Real-time dynamics of lymph-flow velocity in a lymph microvessel, recorded with a laser speckle technique (curve 1) and by processing the video recording (curve 2).

cells)[116,94]. Fluorescent imaging was performed with CCD cameras (Cascade 650, Photometrics, color Nicon DXM1200) and a super-sensitive PentaMAX camera with an intensifier (Princeton Instruments, Inc.).

STUDY OF MICROLYMPHATIC DYNAMICS

Label-free time-resolved lymphography

An essential ingredient in studying the functional activity of lymph microvessels is to know when the observed functions approximate normal conditions. The previously described imaging system allowed us to obtain such basic information on intact lymph microcirculation, including quantitative measurements such as indices of phasic contraction and valve function, the numbers of microvessels with lymph flow, the numbers of cells in lymph, and lymph flow velocity[58,66,101,125].

TDM images of rat mesentery at two relatively small magnifications (4 ×, field of view 250 × 350 μm and 10 ×, field of view 125 × 175 μm) allowed us to visualize the initial (Figure 3F) and valvular lymphatics (Figure 3H), the vessel wall, lymphatic valves, and cells in lymph flow, as well as neighboring blood microvessels. In particular, we studied small valvular lymphatics with mean diameters of 147 ± 3 μm. Half of these lymphatics in a normal state had spontaneous phasic contractions[101].

The rate (frequency) of contractions and contraction amplitude (the percentage difference between maximum and minimum diameters during contraction) vary significantly[66]. Benoit *et al*[22] found that the lymphangions with phasic contractions have mean end diastolic diameters of 69.2 ± 6.5 μm and systolic diameters of 39.4 ± 5.6 μm (i.e. an amplitude of 43%). In another paper, the same authors showed that lymphatics with mean end diastolic diameters of 106.9 ± 13.7 μm have a systolic diameter of 69.8 ± 8.8 μm (i.e. amplitude of 35%)[30]. From our data, lymphangions had mean diastolic diameters of 147 ± 3 μm and amplitudes of 29% ± 9%[58]. Thus summarized, these data indicate that the larger lymphatics have smaller amplitudes of phasic contractions. Our detailed analysis of relationships between diameter and amplitude revealed that the lymphangion with larger diameters have less amplitude

(Figure 8, unpublished), which is in line with the results presented above. In addition, we believe that the amplitude of phasic contractions should be analyzed in relation to valve activity; indeed, the amplitude of phasic contractions in lymphangions with active valves was 31% ± 4%, while in lymphangions with non-active valves it was only 6% ± 2%[66].

The majority of lymphatics with phasic contractions (78%) have active valves, which periodically open and close. An average activity rate (frequency of closing-opening cycles per minute) was 9-12/min[58,66,101,125].

Cells are moved in 85% of lymphangions and they are not found in 15% of lymphangions[66,125]. It is well known that some parts of blood capillaries do not work normally[61]. We speculate that the same situation may occur in lymphatics, in which activity can start under some specific circumstances, for example during disease development (e.g., lymphedema).

Lymph flow velocity is usually estimated by measuring cell velocity. Our measurements with a conventional video camera (25-30 fps) revealed that mean cell velocity in an axial flow in the non-valvular central part of mesenteric lymphangions (i.e. approximately equal distance between input and output valves) is 211-262 μm/s on average, with a maximum of 1-2 mm/s)[58,66,101,125]. When lymph flow goes through the valve, the phase contraction leads to acceleration of flow because of the narrow valve nozzle. In turn, this leads to significantly increased cell velocity.

Lymph usually moves in the forward direction for a short period of time; then, the motion is interrupted and the lymph stops for up to 1-1.5 s. After that, the lymph flow starts in the reverse direction. Usually, cells oscillate at a rate of 50-70 oscillations per minute[126]. Figure 9 shows oscillations during 15 s in a non-valvular part of an individual lymphangion (mean diameter in the investigated site = 170 ± 5 μm; mean cell velocity during the investigated time = 168 ± 6 μm/s)[126]. In some rare microvessels, the time-averaged velocity of lymph flow equaled zero. In this case, lymphocytes only oscillated relative to a position without the leak-back of lymph. Using a high-speed videotape recorder (2000 fps), Sekizuka *et al*[24] demonstrated that maximum cell velocity in rat mesenteric lymphatics was 2-3 mm/s. Later, using a relatively high-speed camera (500 fps), Zaviewa *et al* determined that maximum cell velocity in some mesenteric lymphatics may reach 7 mm/s and their oscillations correlate with phasic contractions[26]. Probably, such variability of cell velocity may result from different experimental conditions.

It is important that the analysis of lymph flow requires that we estimate both cellular and plasma velocities (analogous to blood flow). In fact, Starr *et al*[8] found that the blood flow in cat mesenteric microvessels *in vivo* is characterized by a discrepancy between RBC and plasma velocities. This discrepancy is dependent on the elastic properties of RBCs and flow dynamics, including plasma shear and pressure field. We expect a similar phenomenon in lymph flow, especially due to its oscillating character; however, these effects require further quantitative verification.

Depending on lymph flow velocity and vessel structure, cell distribution in the cross-section of the lymphangion varies[58,66,125]. Most often, at relatively low velocities and/or in the non-active valves (80% of cases), cell distribution was relatively uniform. However, at high velocities and/or in functioning valves (20% of cases), most cells were concentrated near the vessel axis.

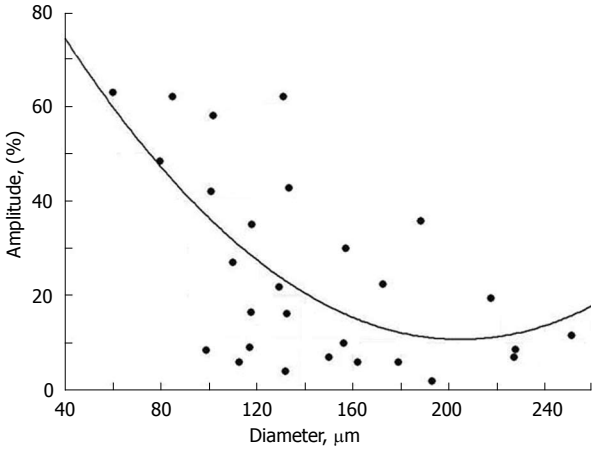

Figure 8 Diameter-amplitude relationship in rat mesenteric lymphangion. Cycles-experimental data, solid curve-approximation (A = 109.3-0.96 × D + 0.0024 × D^2, where A: amplitude and D: diameter).

It is well known that lymph has markedly lower concentrations of cells than blood. However, there is relatively little data about cell concentration in prenodal lymph. In particular, cell concentrations range from 200 to 1000 cells/μL in prenodal sheep's lymph and 100 cells/μL in prenodal rabbit's lymph[127,128]. It was found that approximately 1 × 10^6 cells/h (1.7 × 10^4 cells/min) go through a single prenodal (afferent) sheep's lymphatic[129,130].

According to our data, the cell concentration in rat mesenteric prenodal lymphatics is larger. Specifically, we measured the number of cells in a 50 μm × 50 μm square in the central part of a lymphangion from a rat mesenteric microvessel using 2D-imaging[66]. Because the depth of field was approximately 28 μm, the number of cells was determined in a 50 μm × 50 μm × 28 μm volume (i.e., 7 × 10^{-5} μL of lymph). Data is summarized in Table 1 (taking into account distribution of cells in a cross-section of a lymphangion, see above). Finally, the mean concentration of cells in the lymph flow of intact mesenteric microvessels was estimated as approximately 0.5-1 × 10^5 cells/μL. From these data, the average percent of cell fraction in lymphatics was 5.5%. This parameter is analogous to hematocrit in the blood system, and may be called lymphocrit. It is interesting that a 5%-6% level of hematocrit can be found only in blood capillaries, as compared to that in arterioles with diameters from 60-70 μm, in which the hematocrit achieved 20%-30%. Cell flux in the prenodal lymph was estimated to be 10-50 cells/s. The cell concentration in flow is usually higher in vessels with higher lymph flow velocities, and is somewhat correlated with the amplitude of phase contractions and rate of valve activity[66]. Recent data obtained by Dixon *et al*[131] with a high-speed video system and by capturing multiple contraction cycles in rat mesenteric lymphatic preparations with smaller diameters (91 ± 9 μm) revealed that lymphocyte densities were 12 000 ± 5200 cells/μL

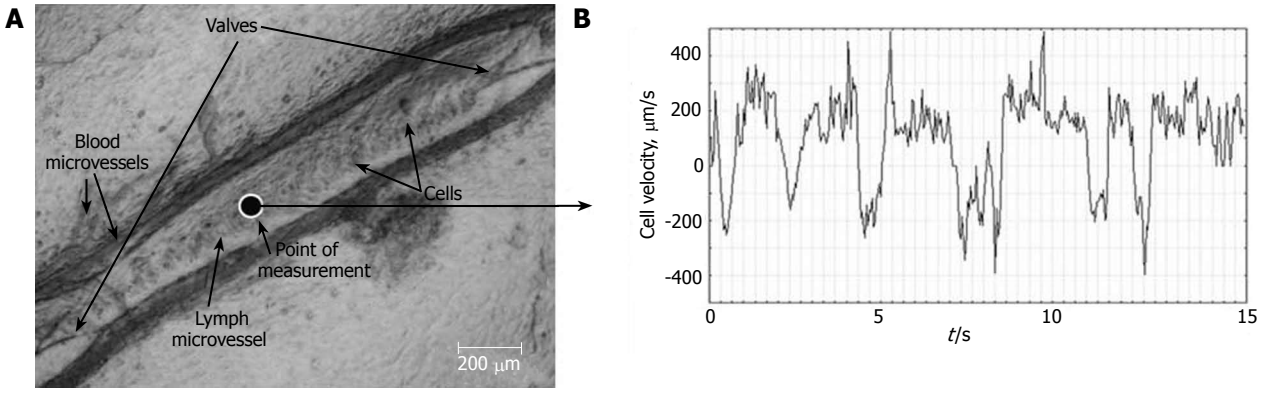

Figure 9 Real-time dynamics of cell velocity in axial lymph flow within the non-valvular segment of a lymphangion (mean diameter of 170 ± 5 μm) without phasic contractions and valve activities, measured by processing the video recording (μm/s) for 15 s.

Table 1 Relationship between lymphocrit and other parameters of microlymphatic function

	Cell concentration, cells/μL	Lymphocrit %	Proportion of Lymphangions %	Diameter μm	Parameters of phasic contractions		Valve activity per minute	Cell velocity (μm/s)
					Amplitude (%)	Count of contractions per minute		
Group 1	$< 3.75 \times 10^4$	< 2	22	$106 \pm 9^{a,b}$	$50 \pm 15^{a,b}$	12 ± 2	8 ± 0.5^{b}	161 ± 191
Group 2	3.75×10^4-12.2×10^4	2-6	45	141 ± 8^{a}	$28 \pm 7^{a,c}$	12 ± 1	11 ± 1	254 ± 151
Group 3	$> 12.2 \times 10^4$	> 6	33	165 ± 9^{b}	$14 \pm 5^{b,c}$	15 ± 1	16 ± 2.5^{b}	214 ± 19

$^{a}P < 0.05$, *vs* Group 2; $^{b}P < 0.05$, *vs* Group 3; $^{c}P < 0.05$, *vs* Group 3.

and cell flux was 990 ± 260 cells/min.

The relationship between lymphocrit and pathologies is still unknown. There are indications that the leg massage of healthy rabbits stimulates lymph flow and increases cell concentration, while leg edema due to venous pressure rising is not accompanied by an elevation in cell concentration[128].

Data about cell composition in afferent lymph are very limited and have been obtained in *in vitro* tests. In particular, 80%-90% of cells in normal prenodal lymph are related to mature lymphocytes, 5%-20% to macrophages and dendritic cells, and 0%-10% to other cells (e.g. basophilic blast cells, RBCs)[127]. The composition of WBC types changes based upon the pathology. For example, it is estimated that there is a significanct appearance of neutrophils in experimental peritonitis in sheep. Other important problems are the mechanisms by which different cells (e.g. metastatic tumor cells) enter into peripheral lymphatics. Recently, Azzali studied tumor-associated absorbing lymphatics in the peritumor area of fixed tissue specimens (adenocarcinoma, melanoma, colorectal cancer) using light microscopy, transmission electron microscopy, and histochemistry with 3-D image reconstruction[132]. He found that cancer cells can enter into lymphatics through intraendothelial channels (1.8-2.1 μm in diameter and 6.8-7.2 μm in length). These results are very promising, but such a mechanism remains to be proven in living cells *in vivo*.

Lymph and blood flow cytometry in vivo

We demonstrated the first application of the PT techniques for lymph and blood PT flow cytometry (PTFC) *in vivo* integrated with TDM[94,115,116,133]. To minimize cell image distortion due to spatial cell-radial fluctuations in lymph flow (up to 50 μm in 150-μm-diameter lymph vessels), cells were imaged immediately after passing through a lymphatic valve, which played the role of a natural nozzle, focusing the cells near the vessel axis (Figure 3J). Thus, lymphatic valves provided a natural type of "hydrodynamic focusing" (a term used in *in vitro* FC involving an artificial nozzle) to limit lateral fluctuation of cells up to a few micrometers.

High-resolution and high-speed TDM imaging provides a real-time monitoring of individual cells in blood (Figure 3L-N) and lymph flow (Figure 3I-K), as well as static and migrating cells in the interstitium (Figure 3O), lymph nodes (Figure 3A and B), and even in liver (Figure 3C)[58,94]. The high spatial resolution offered by TDM (300-500 nm at 40× - 100× magnification with water immersion) makes it possible to identify some types of moving cells based upon their sizes and shapes (e.g. WBCs and RBCs; Figure 3K). We can even monitor the rotation of a single RBC (Figure 10A-C) and visualize intralymphatic cell aggregates of different sizes in intact microlymphatics (Figure 10D-F).

PT module in integrated FC allows us to obtain PT images of flowing cells (e.g., lymphocytes, RBCs, and leukemic cells) with an absorption sensitivity approximately four orders of magnitude greater than the sensitivity of transmittance microscopy (Figure 3K, left and middle columns)[94]. In particular, PT images revealed the subcellular structures of these cells (Figure 3K, middle column) associated with the spatial distribution of cytochromes in lymphocytes and cancer cells and of hemoglobin in RBCs, which were not clearly visible with

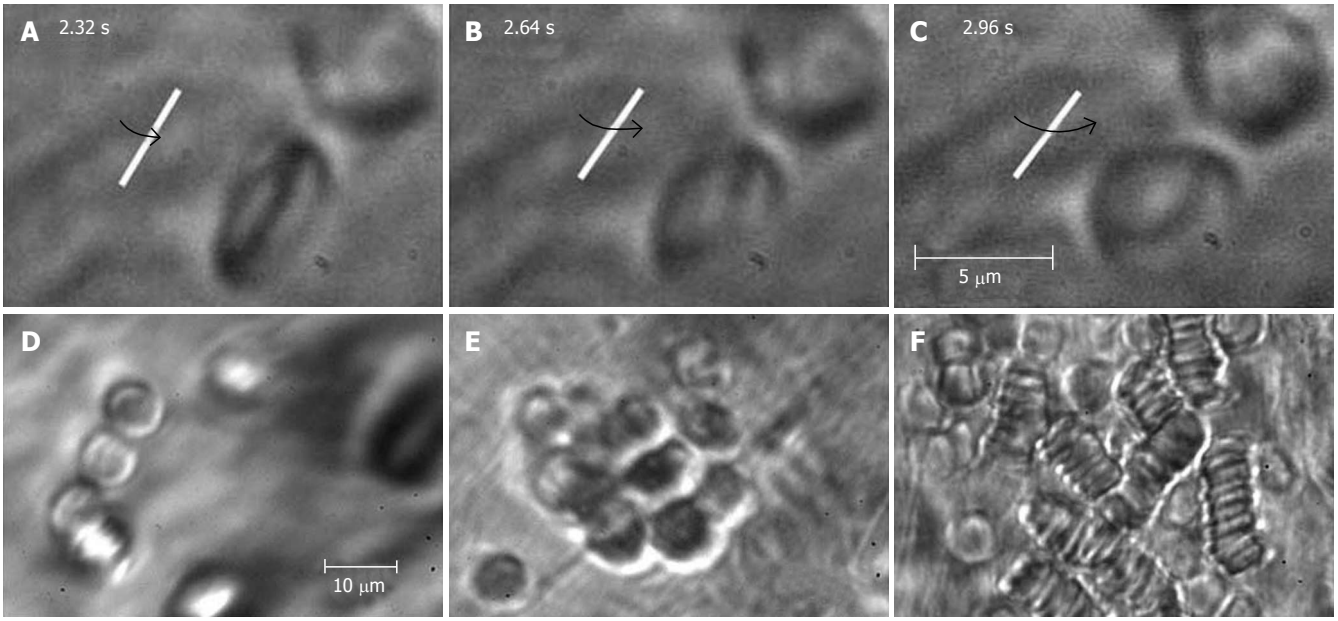

Figure 10 High-resolution monitoring of cell behavior in lymph flow. Top row (**A**-**C**): three sequential images of an individual RBC's rotation in lymph flow (lymphatic diameter 185 μm, mean cell velocity 220 μm/s, magnification 100 ×). Bottom row: moving aggregates of different sizes in lymph flow; **D**: Unstable aggregate of a few cells in intact lymphatic; **E**: large aggregate of RBCs in lymph flow resulting from venous insufficiency; **F**: rouleaux formation when numerous RBCs appeared in lymph flow due to laser-induced hemorrhage (magnification 100 ×).

TDM (Figure 3K, left column). Fluorescence images, obtained with a high-sensitivity CCD camera with an intensifier (PentaMAX, Princeton Instruments, Inc.), showed high image contrast (Figure 3K, right column) similar to that of PT images, although inconvenient staining procedures were required. Specifically, leukocytes were labeled with Rhodamine 6G. RBCs and K562 cells were labeled with FITC and MitoTracker Red, respectively. Because of differences in the optical properties of normal and cancerous cells, especially mitochondrial distribution[134,135], which can be visualized with the PT technique, we can assume that PTFC has the potential to distinguish these cells after further improvements.

PT-signal tracings from flowing cells in blood (Figure 11A) and lymph (Figure 11B-E) microvessels were obtained as a function of time[116,94] . Due to their different absorption properties, the significant (40-60-fold) differences in the integral PT amplitudes from RBCs and WBCs (lymphocytes) allowed us to distinguish cells using only the thermolens mode (i.e. even without imaging). Cells were also identified through differences in cooling times (6-10 μs for RBCs, and 20-25 μs for lymphocytes). PT signals from RBCs in blood flow showing a purely positive component indicate a linear positive PT response from the cells at a low laser energy level with no cell damage (temperature increase is usually 5-10℃, Figure 11A). The amplitude differences indicate differences in average absorption and reflect the natural heterogeneity of RBCs. The negative signal component from cells in lymph flow presented in Figure 11D is related to laser-induced photodamage through bubble formation around strongly absorbing cellular zones that have been overheated. The presence of both positive and negative components in the PT-signal amplitude tracing (Figure 11E) indicated a noninvasive condition for lymphocytes (which have a high photodamage threshold) and an invasive condition for RBCs (which have a low photodamage threshold) at the same energy level. Decreasing the laser energy level

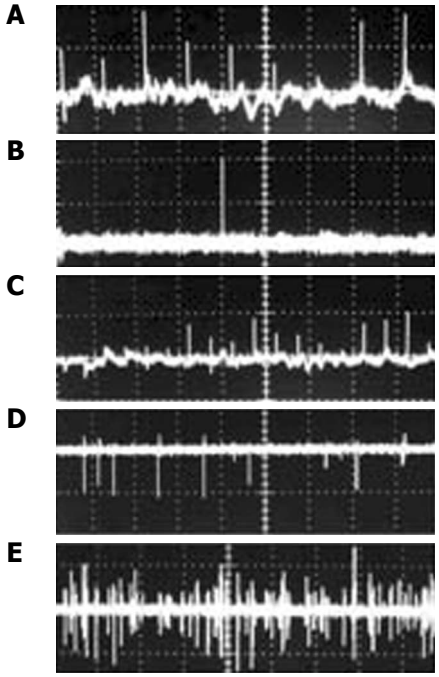

Figure 11 Typical PT-signal tracings from blood cells in blood and lymph flow: **A**: RBCs in blood flow; **B**: rare RBC in lymph flow; **C**: growing number of RBCs in lymph flow during laser-induced hemorrhage; **D**: laser-induced damage of RBCs in lymph flow and lymphocytes in lymph flow in linear and nonlinear PT modes; and **E**: lymphocytes and RBCs in lymph flow. Laser parameters: wavelength, 525 nm; energy/amplitude/time scale/division: (**A**), 0.3 μJ/50 mV/100 ms; (**B**), 0.5 μJ/20 mV/1 s/div; (**C**) 0.6 μJ/100 mV/200 ms/div, (**D**) 5 μJ/500 mV/4 s/div; and (**E**) 145 μJ/100 mV/10 s, respectively.

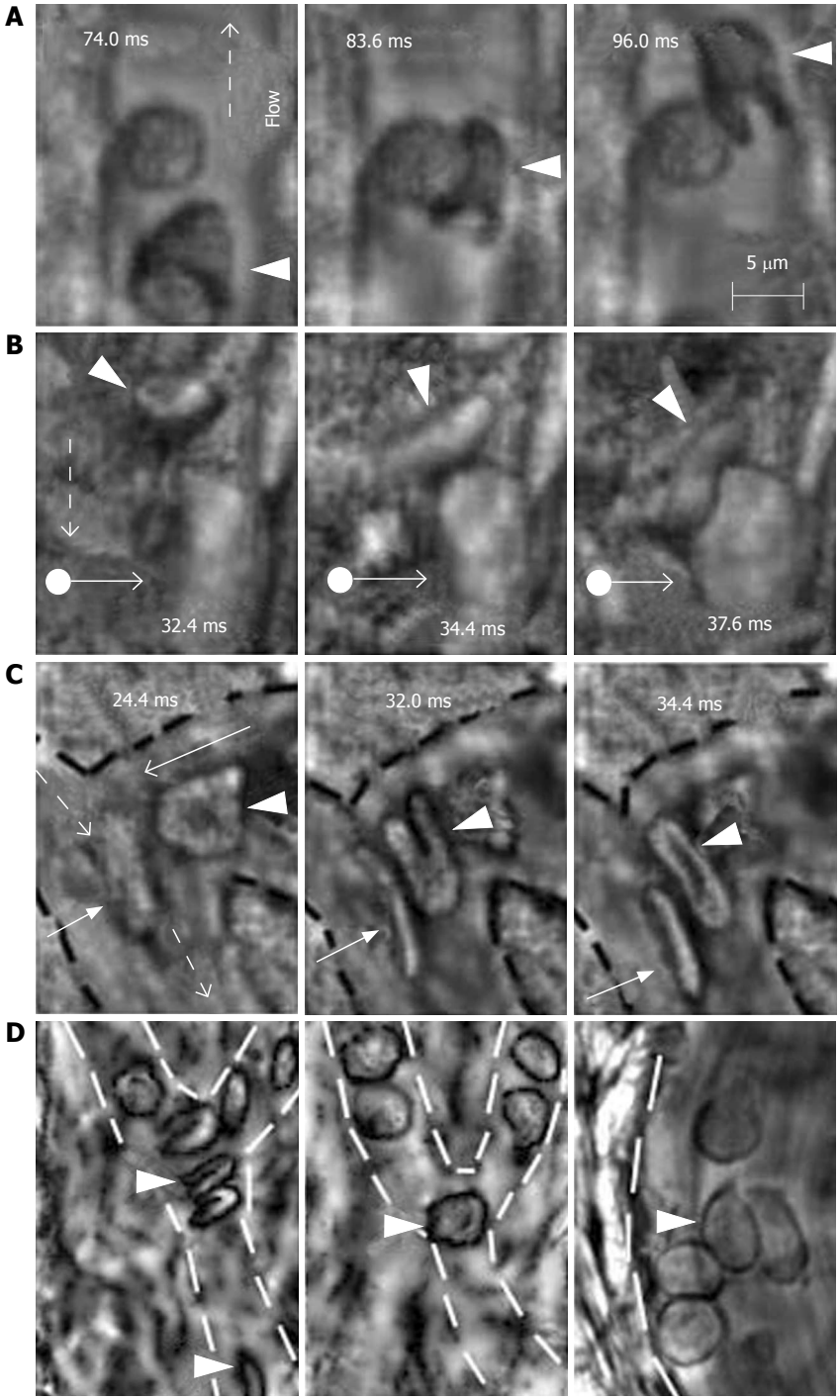

Figure 12 High-resolution, high-speed monitoring of cells in blood flow. RBCs are indicated by conventional arrows and triangle; rolling WBCs by arrows originating from filled circles; and direction of flow by dashed lines. **A**-**C**: behavior of normal RBCs and WBCs in flow (1250-2500 fps; 40 ×); **D**: The shapes of normal (left) and diamide-treated (middle) RBCs in single-file flow of small venula (diameter ~10 μm), and (right) adhesion of diamide-treated RBCs to wall of the relatively large venula (diameter -40 μm).

allows us to selectively identify rare RBCs in lymph flow. For example, Figure 11B shows the detection of single RBCs at a low laser energy level. This level did not produce notable PT signals from the many lymphocytes in lymph flow because of their low absorption. Laser-induced vessel injury led to a fast-growing number of RBCs in lymph flow (Figure 11C). The next tracing shows that the PT signals from RBCs at a relatively high laser energy level led to cell damage (Figure 11D).

HIGH-SPEED IMAGING OF INDIVIDUAL CELLS IN FAST BLOOD FLOW

This technique, using an advanced high-speed CMOS camera, reveals the high deformability of parachute-like RBCs as they are squeezed at 0.6 mm/s through a narrow gap between the vessel wall and rigid adherent cells on the opposite wall (Figure 12A)[104]. It also shows how quickly the relatively fast-flowing RBCs (~1 mm/s) change shape as they interact with the much more slowly moving (so-called rolling) leukocytes (~0.1 mm/s; Figure 12B). We also observed significant dynamic deformation of two RBCs in merging flow streams in a bifurcation zone (Figure 12C), and extremely fast stretching (0.4 ms at 2500 fps) of initially discoid RBCs to ~0.7-0.9 μm (Figure 3N). Our technique has provided relatively good contrast images of both slow- (20 μm/s, Figure 3L, left) and fast-flowing (2.5 mm/s) single platelets in blood microvessels. The best-quality images of platelets were obtained in the RBC-free

space of the microvessel lumen.

We also performed time-resolved monitoring of cell deformability. In particular, diamide (20 mg/kg) was injected in a rat's tail vein to increase the rigidity of RBCs *in vivo*. We observed a drug-induced decrease in the deformability of RBCs in fast blood flow (up to 5 mm/s) compared to RBCs in normal conditions, with maximum centrifugal forces acting on cells in curved capillaries (Figure 12D, left and middle). In addition, diamide led to adhesion of abnormal RBCs to vessel walls (Figure 12D, right). To our knowledge, this was the first time that these phenomena have been observed with high-speed, high-resolution imaging *in vivo*. After additional study, potential applications of this technique may include fundamental studies of dynamic cell-cell interactions in native flow or the identification of abnormal cells (e.g., cancerous cells or sickle RBCs) using their different dynamic deformability as new biological markers that are sensitive to disease development or to different interventions.

IMAGE CYTOMETRY OF STATIC CELLS AND TISSUE STRUCTURES

Interstitium

Figure 3O shows typical high-resolution TDM images of mast cells, adipocytes, and slow-moving RBCs in mesenteric interstitium[58,101]. This technique also provides distinct images of fibrils, as well as other static and migrating cells. In some cases, the phase-contrast images demonstrated better contrast of margins and sub-cellular structures for selected single cells in interstitium than does non phase-contrast at high magnification (100 ×, with water immersion), which prevents overlapping refractive heterogeneities of connective tissue (see images of mast cell and adipocytes in Figure 3O).

Lymph and blood microvessel walls

With TDM, we obtained high-resolution images of (1) distinct individual blood endotheliocytes (EC) of the capillary wall (Figure 3L, left); (2) the initial lymphatic wall with cells (e.g. leukocytes) migrated from interstitium (Figure 3G); and (3) lymphatic wall and valvular cusp structures of larger vessels[58].

Lymph node

Using a minimally invasive procedure, we demonstrated real-time, *in vivo* monitoring of individual cells in different domains of mesenteric lymph nodes (e.g., medullary sinus, light and marginal zones of marginal sinus) in their native state (unpublished data, Figure 3B)[94].

STUDY OF ENVIRONMENTAL IMPACTS ON LYMPHATICS

To date, the effects of environmental and therapeutic interventions on blood microcirculation have been studied in appropriate detail in humans and in different animal models, including the rat mesentery; however, the lymphatic system has received much less attention in spite of the many biological and medical problems associated with microlymphatic functioning and its disturbance in different diseases, including cancer metastasis, venous insufficiency, infections, inflammation, lymphatic malformations, and especially lymphedema[29,40,62]. To partially fill this knowledge gap, we used a rat model with an integrated optical technique to quantitatively study lymph and blood dynamics under different impacts, including chemical, drug, and physical interventions. In our study, we chose interventions that have effects on lymphatics that are unknown (dimethyl sulfoxide); incompletely known (β-adrenoceptor agonist and β_1- and β_2-adrenoceptor antagonists, donors of NO, low-power laser radiation); or controversial (inhibitors of NO-synthase). These effects were studied by real-time monitoring of the diameters and parameters of phasic contractions, and changes in lymph flow velocity, valve activity, and cell behavior in microvasculature.

Effects of adrenergic agonists and antagonists

One of the most important regulators of the vasculature is adrenergic regulation through α- and β-adrenoreceptors[61]. The effects of adrenergic agonists and antagonists on diameter and phasic contractions of microlymphatics have been described in *in vitro* or *in vivo* tests[22,29,30]. It is known that norepinephrine applied topically or injected intravenously instantly reduces the diameter and increases the contraction frequency of rat mesenteric lymphatics, while isoproterinol has opposite effects[29]. Moreover, the attempts to study the effects of α-adrenoagonists and antagonists on lymph flow in microvessels were made using calculated parameters of lymph outflow (as calculated with the following assumptions: strongly cylindrical, unchanging geometry of lymph vessel with unidirectional lymph flow)[22,30]. It was shown that α-adrenergic regulation of lymph outflow in mesenteric lymphatics is through α_1-receptors[30].

In our tests, we clarified the effects of a β-adrenoceptor agonist and antagonist (and their subtypes) on cell flow velocity *via* the direct monitoring of lymph flow, and determined the relationships between cell velocity and other parameters of microlymphatic function (diameter, amplitude and rate of phasic contractions, rate of valve activity) (Table 2). Isoprenaline, a β-adrenoceptor agonist, (10^{-5} mol/L, 15 min of topical application) caused dose- and time-dependent responses: 5 min following topical application, the percentage of contracting lymphangions was decreased from 60% to 33% and lymph flow velocity was inhibited from 134 ± 13 μm/s to 82 ± 19 μm/s ($P < 0.05$). Then, at 15 min, 40% of lymphangions exhibited lymphostasis accompanied by vessel constriction and depression of phasic activity. The adrenoceptor antagonists metoprolol (β_1) and butoxamin (β_2) were also applied topically at the same parameters (10^{-5} mol/L, 15 min). Both antagonists stimulated phasic contractions in non-active lymphangions. However, the effect of metoprolol was more marked, increasing the proportion of microlymphatics with contractile activity to 66%, while butoxamin stimulated phasic activity in only 32% of non-active lymphangions. As a result, metoprolol's action significantly increased lymph flow velocity (from 136 ± 14 μm/s to 198 ± 24 μm/s, $P < 0.02$), while it did not change with butoxamin. Based upon this data, we assume

Table 2 Effects of 15-min topical application of different vasoactive drugs on lymph microvessel functions

Drug	Diameter	Phasic activity	Lymph flow velocity
Sodium Nitroprusside (10^{-5} mol/L)	Dilation	Slight short-time inhibition	Unchanged
N-Nitro-L-Arginine (10^{-4} mol/L)	Unchanged	Stimulation	Stimulation
Isoprenaline (10^{-5} mol/L)	Constriction	Inhibition	Inhibition up to stasis
Metoprolol (10^{-5} mol/L)	Unchanged	Stimulation	Stimulation
Butoxamin (10^{-5} mol/L)	Unchanged	Slight stimulation	Unchanged
Dymethyl Sulfoxide, (30%)	Constriction	Stimulation	Stimulation in 50% of lymphangions
			Inhibition in 39% of lymphangions (without phasic contractions)

Table 3 Effects of 30% DMSO at the topical application on blood microvessel diameter

	Arterioles			Venules	
Before application	16.5 ± 0.49	25.3 ± 0.69	16.1 ± 0.79	24.9 ± 0.74	34.8 ± 0.66
After DMSO application					
1 min	17.4 ± 0.67	25.8 ± 1.09	18.6 ± 0.98[a]	29.6 ± 1.29[a]	39.0 ± 2.25
2 min	16.9 ± 0.83	28.1 ± 0.80[a]	19.2 ± 1.11[a]	28.9 ± 1.33[a]	38.8 ± 1.53[a]

Significant differences from state before application, [a]$P < 0.05$.

that lymph microvessels (and probably similar large lymph vessels), have β_1- and β_2- adrenoceptors.

No effects

Another essential regulative substance of lymph mesenteric microvessel function *in vivo* is nitric oxide (NO)[35,66,136,137]. According to our data, intravenous injection of an NO donor (sodium nitroprusside, 100 μg/kg, i.e. drug concentration in blood is 5×10^{-5} mol/L) caused slight dilation of lymphatics within 30 min[136]. However, sodium nitroprusside does not affect lymph flow. The response of lymphatics to direct topical application of sodium nitroprusside (10^{-5} mol/L, 30 min) was similar but more intense: dilation of lymphangions for 25 ± 2.5 μm was accompanied by slight transient inhibition of the proportion of lymphatics with phasic contractions and active valves[137].

While the hyper-production of NO does not change lymph flow, the inhibition of NO synthesis stimulated lymph motion (Table 2). Topical application of N-nitro-L-arginine, a known inhibitor of NO (10^{-4} mol/L, 30 min), first caused (fifth minute of application) a short-term decrease in the amplitude of phasic contractions (from 23% ± 3% to 11% ± 1%, $P < 0.001$) and stimulation of valve activity (rate of valve activity increased from 6 ± 1 to 11 ± 2 per min, $P < 0.05$)[66,137]. Then, from the tenth minute, we observed permanent stimulation of phasic activity and lymph flow. Shirasawa and coauthors concluded that a 15-min application of an NO donor and an inhibitor of NO synthase portray the direct effects of NO on microvessel walls[35]. Therefore, we speculate that NO can regulate lymph flow in microvessels due to (at least, partly) the direct action of NO on the endothelium and the smooth muscles of lymph microvessel walls.

Pharmacological effects of dimethyl sulfoxide (DMSO)

DMSO has a wide spectrum of biological activities, including high penetrating activity and significant vasoactive effects on blood vessels[138,139]. It is used for local treatment of trauma, arthrosis, and rheumatoid arthritis[140,141]. The effects of DMSO on the microlymphatic system are unknown. Experimental studies have revealed that a 30-min topical application of 30% DMSO caused specific, dynamic microvascular changes in blood and lymph[66,142]. Immediately after application (within the first minute), there was stasis within 100% of venules and 85%-95% of arterioles, with significant dilation (dilation began earlier and the diameter increased more in venules than in arterioles) and hemorrhaging around venules (Table 3). The marked responses of lymphatics started later (15 min of DMSO application), and appeared as a significant increase in lymph-flow velocity from 190 ± 12 μm/s (before DMSO application) to 233 ± 20 μm/s ($P < 0.05$) accompanied by stimulation of phasic contractions in 21% of lymphangion and decreasing of diameter. In parallel, the 39% of lymphatics is characterized by lymphostasis development (Table 2). Obtained on DMSO' s impacts on lymph and blood microvascular function can be used for assessment the possible side effects of this drug.

Effect of low-power laser irradiation

Publication of the positive clinical effects of low-power laser therapy, including lymphedema treatment, stimulated our interest in studying lymphatic response to this radiation[143-145]. The effects of low-power laser radiation (He-Ne laser) on intact lymph microvessels were studied at three radiation intensities-450 mW/cm^2, 45 mW/cm^2, and 14 mW/cm^2-each with an exposure time of 15 min[66,136,146]. Laser power of 14 mW/cm^2 did not have a significant effect on lymph microvessel function. After 5 min of irradiation at 45 mW/cm^2, 70% of lymphatics were dilated an average of 8 ± 1 μm ($P < 0.01$). After 15 min, the proportion of microvessels

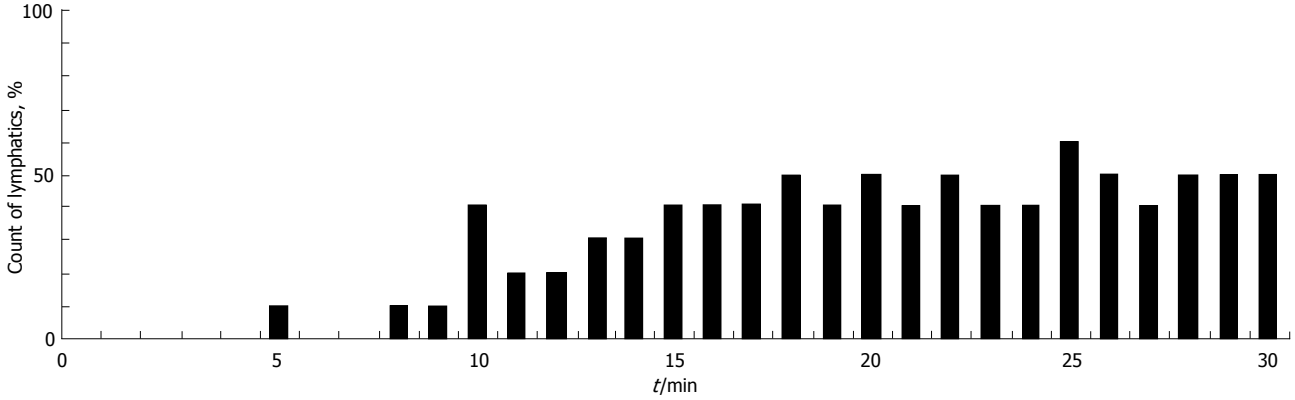

Figure 13 The percentage of lymphangions exhibiting phasic contractions during 30 min of irradiation with a He-Ne laser (450 mW/cm^2).

that were dilated (60%-70%) did not change, and phasic contractions appeared in 21% of lymphatics. When the lymphatics were irradiated at the highest laser power (450 mW/cm^2), similar dilation of the majority of microvessels was observed. Simultaneously, 15 min of laser radiation at 450 mW/cm^2 significantly stimulated contractions within a larger number of vessels (45%) than did irradiation at 45 mW/cm^2. The mean contractile amplitude of irradiated vessels was 1.5-fold greater than that of intact lymphatics (44% ± 5% compared to the amplitude of spontaneous contractions of 29% ± 9%). Increasing the irradiating time up to 30 min at 450 mW/cm^2 did not change the degree of lymphatic dilation and just slightly increased the proportion of lymphatics with phasic contractions (Figure 13). These laser effects were maintained up to 30 min after irradiation. None of the doses of laser radiation affected how the valve functioned. Thus, our data is in line with the results of Carati *et al*[32] in that low-power laser radiation may improve lymph drainage by stimulating phasic contractions and by dilation of microvessels.

High-power laser treatment of vascular abnormalities

Rat mesentery microvasculature is very useful as a model for laser treatment of port-wine stains and other vascular abnormalities. In particular, in one study, rat mesenteric blood vessels were irradiated with a laser pulse (585 nm, 0.2-0.6 ms pulse duration, 0.5-30 J/cm^2 radiant exposure)[147]. Video microscopy was used to assess vessel dilation, formation of intravascular thrombi, bubble formation, and vessel rupture. Changes in reflection during a laser pulse were measured by simultaneously recording the temporal behavior of the incident and reflected light. A threshold radiant exposure of approximately 3 J/cm^2 was found to produce changes in the optical properties of blood *in vivo*, confirming previous *in vitro* results. Often, laser exposure induced a significant increase in vessel diameter, up to three-four times the initial diameter within 200 ms after laser exposure. Sometimes, immediately after the pulse, round structures, interpreted as being gas bubbles, were seen within the vessel lumen.

We obtained similar results in our study with a 10 ms laser pulse (585 nm, 0.5-30 J/cm^2 radiant exposure). In addition, local hemorrhaging around venules with rupture of venular walls occurred at lower radiant exposures than in arterioles with smaller diameters (due to the more effective cooling effects in smaller vessels; Figure 14A and B). For the first time, significant constriction of neighboring lymphatics was observed, up to obliteration of lumina and lymph stasis (Figure 14C and D). Additionally, hemorrhage in the interstitium led to the entry of many RBCs (visualized as distinct red points by TDM) into the lymph flow. The PT mode of integrated PTFC proved this fact. In particular, PT-signal tracing specific for RBC laser energy levels showed a growing number of RBCs in lymph flow during laser-induced hemorrhage (Figure 11C).

Preliminary data from intravenous injection of 100-nm gold nanoparticles followed by laser irradiation of the mesentery demonstrate a decrease in the blood vessel damage threshold (approximately 3-5 times) compared to the damage induced without nanoparticles, despite the sub-optimal parameters of the laser used [wavelength was outside the maximum absorption of the nanoparticles (~525 nm), and of relatively long pulse duration]. Nevertheless, to our knowledge, this was the first demonstration of the application of nanotechnology to treat blood vessels with laser-activaded gold nanoparticles and their nanoclusters[148-154].

Combined action of laser and drugs

Sodium nitroprusside increased the sensitivity of lymph microvessels to low-power He-Ne laser radiation[136]. After intravenous injection of sodium nitroprusside (100 μg/kg), application of He-Ne laser radiation at the lowest power (14 mW/cm^2 for 15 min) stimulated phasic contractions in 44% of lymph microvessels against a background of stable dilation caused by the drug. Contractions occurred at a rate of 6-25/min and had amplitudes of 8-22 μm. In comparison, this dose of laser radiation alone had no notable effect on the phasic contractions of intact microvessels. Such an approach could have great potential for developing innovative therapies for some diseases (e.g., lymphedema).

Nicotine intoxication

Nicotine, an important component of cigarette smoke, was shown to be indirectly responsible for inducing

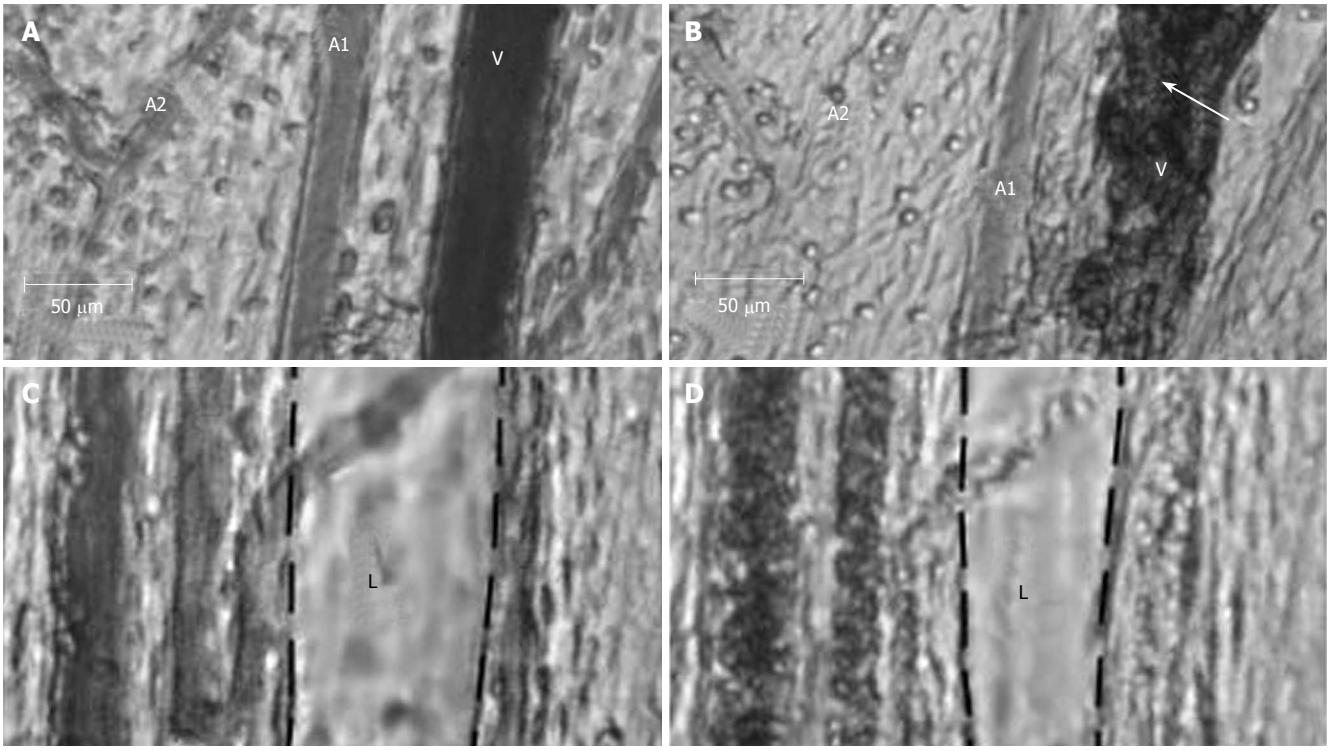

Figure 14 Effect of a laser pulse (585 nm, 10-ms pulse duration, 0.5-30 J/cm^2 radiant exposure) on blood and lymph microvessels *in vivo*. **A**: Intact venule (V) and arterioles (A1 and A2) with good blood flow; **B**: Damage to these microvessels immediately after laser pulse: local hemorrhage (arrow) around the venule (V) and stasis in a small arteriole (A2); **C**: Intact lymphatic (L) before laser pulse (black dash line shows internal margin of lymphatic wall); **D**: Laser-induced constriction of the lymphatic, which coincided with stasis in neighboring venules.

pathology in many tissues, both human and animal[155-157]. Exposure to cigarette smoke increases the nicotine level in the blood to a maximum in less than 10 s. Therefore, the immediate responses of the vascular network to the action of nicotine appear to be important in the development of acute pathology. The pathological effects of nicotine on blood microcirculation have been reported in sufficient detail, but its impact on the lymphatic system remains obscure.

We uncovered the first experimental evidence of potential active participation of lymph microvessels in the mechanisms of nicotine's effects *in vivo*[158]. The influence of nicotine on microlymphatics was determined using three routes of nicotine administration: (1) direct topical application in various concentrations (0.001 mmol/L, 10 mmol/L, and 100 mmol/L solutions) for 15 min; (2) acute injection of nicotine solution (10 mmol/L) through a cannulated vein; and (3) chronic administration for 14 d *via* subcutaneous injection from a mini-osmotic pump (10 mmol/L solution; 0.5 μL/h delivery rate).

The topical application showed that the most significant responses of microlymphatics to nicotine's impact were at 10 mmol/L and 100 mmol/L doses. In particular, the concentration of 10 mmol/L caused a significant, immediate short-term (12-40 s) constriction of 100% of the lymphangions. The effect started within 3-5 s of application (67% of cases) or after ~3 min of nicotine exposure (33% of cases). The lymphatic diameter was decreased by 34% ± 7% (more than ~2 times the amplitude of spontaneous phasic contractions before nicotine application). In all cases with the highest concentration of nicotine (100 mmol/L), the same immediate constrictions were associated with the slowing of lymph flow, local stable constriction of lymph microvessels, asynchronous motion of the lymphatic wall, stasis in blood microvessels, and disturbances of respiration. Thus, under the direct impact of nicotine, there were significant changes in small lymphatic function *in vivo*, which were dose and time dependent. We hypothesize that the obtained effects were the result of the direct action of nicotine on lymph microvessels and probably reflect specific endothelial dysfunction and/or injury of the contractile ability of the lymphatic wall.

Acute nicotine intoxication delivered intravenously slightly relaxed the lymphatics and was sometimes accompanied by slowing of lymph flow and short-term stasis in blood microvessels. Chronic intoxication using a 10 mmol/L concentration (effective at the topical application) did not markedly change the function of lymphatic and blood microvessels and did not differ markedly from that in the intact state. The absence of effects may be the result of adaptation of the microcirculation to the action of nicotine.

Thus, nicotine induces marked changes in small lymphatic function *via* its acute, direct impact *in vivo*. The observed microlymphatic disturbances due to the action of nicotine may be an important mechanism in the complex, immediate reaction of a healthy organism to cigarette smoke. The acute lymphatic damage caused by nicotine could be more crucial in some pathologies or treatments, and suggests that nicotine may contribute to vascular abnormalities and tissue edema.

EXPERIMENTAL MODELING OF DIFFERENT PATHOLOGIES

Damage to lymph microcirculation is an important mechanism underlying the development of many diseases (e.g., tumor, inflammation, infections, intoxications, lymphedema, lymphatic malformation) and often determines their severity[29,40,62,159]. Because rat mesentery is a highly informative *in vivo* model for functional analysis of lymph microdynamics, this animal model was used by us to study the mechanisms of microlymphatic disturbances resulting from different pathologies, such as models of staphylococcal intoxication, pathological stress, lymphedema, and venous insufficiency.

Staphylococcal intoxication

It is well known that α-toxin (α-hemolysin) is the protein produced by *Staphylococcus aureus* and causes serious blood circulatory disturbances with its appearance in blood during staphylococcal diseases; however, its effect on lymph microcirculation is still poorly understood[160-162]. In our study, we used an exotoxic complex (ETC) produced by culture *Staphylococcus aureus* O-15[66,142,163-166]. The main component of this complex is α-toxin (titer ~ 1:640); additionally, it contains a small amount of δ-toxin (titer ~ 1:64). Endotoxins, enterotoxins, and protein A are completely absent.

The staphylococcal intoxication was introduced by intravenous injection of ETC (0.2 mg/100 g) into the tail vein, after which we monitored microcirculation for 30 min. This dose caused serious intoxication. Animals with acute exotoxic shock (those dying within 30 min of ETC introduction) were excluded from the analysis. Disturbances of lymph microcirculation began immediately; after 1 min, the diameters of 75% of the lymphatics were slightly decreased (by 7 ± 2 μm). Between the fifth and tenth minutes of observation, in parallel with vasoconstriction, ETC induced pathologic phasic contractions, characterized by asynchronous wall motion, in half of the lymphatics. After 30 min, lymphatic disturbances were expanded by the development of lymphostasis in 53% of cases.

The resulting effects were due primarily to the direct action of the toxic complex on the lymphatics, as the topical application of ETC in the investigated microlymphatics caused similar microvascular disturbances during a 60-min period. In particular, after a short latent period (58 ± 9 s), ETC induced marked decreasing of lymphangion diameters (36 ± 11 μm from the initial diameter) and stimulated pathologic phasic contractions in 60% of cases. Pathologic phasic activity is characterized by irregular motion of lymphatic walls and defective relaxation (after contraction, the diastolic diameter is sometimes less than it was before). We observed simultaneous abnormalities in blood microvasculature (slowing down of blood flow in venules; increasing migration of leukocytes through venular walls into tissue; and local accumulation of leukocytes around blood microvessels and, as a result, compression of venules into irregular shapes). From the thirtieth to the sixtieth minute of observation, the pathologic constriction of lymph microvessels progressed to complete obliteration of the lymphatic lumen, inhibition of phasic contractions, and gradual development of lymphostasis in 90%-98% of lymphatics. In parallel, we observed blood flow slowing up to stasis and small hemorrhages around venules.

The underlying mechanisms of microlymphatic disturbances include the well-known ability of α-toxin to form the specific Ca^{2+} channels in cell membranes and, correspondingly, to disturb the transport Ca^{2+} in the smooth muscles of the vascular wall and, probably, in the pacemaker cells[167,168]. Thus, these data revealed that an important mechanism of staphylococcal vascular disturbances is damage to the lymph microcirculation. Therefore, therapies for staphylococcal pathology require the correction of microlymphatic dysfunction.

Pathologic effects on lymph microvessels are partially reversible by He-Ne laser radiation and some vasoactive drugs (Euphyllin, Verapamil, DMSO)[66,142,165,166]. In particular, irradiation of the mesentery (450 mW/cm^2 during the first 15 min following ETC application) attenuates typical toxin constriction. In contrast, preliminarily irradiating *in vitro* ETC (20 mW/cm^2, 60 min) attenuates development of lymphostasis: a 60-min application of non-irradiated ETC causes lymphostasis in 88% of lymphangia, while irradiated ETC led to lymphostasis in 57% of lymph microvessels. Thus, low-power laser radiation can attenuate lymphotoxic action *via* its effect on microlymphatic walls, as well as on the properties of ETC itself[166].

However, the most effective corrections of microlymphatic disturbances can be achieved by DMSO. It has been noted above that the effects of DMSO after ETC application (dilation of lymphatics, inhibition of pathologic phasic activity, restoration of lymph flow) are different from the effects on intact lymphatics. Moreover, these local, positive effects are associated with an increase in the duration of animal life, which has been demonstrated in experiments on mice injected with lethal doses of ETC[66,142,165].

Study of experimental lymphedema

Lymphedema is a complication of lymphatic drainage decompensation that may happen during congenital lymphatic dysplasia, hepatic cirrhosis, venous insufficiency, obstruction or surgical extirpation of lymph nodes[159,169,170]. In particular, post-mastectomy lymphedema (PML) develops in 25%-50% of cases after breast cancer treatment[171]. Generally, lymphedema damages the local lymphovascular network (e.g. in affected extremities) causing insufficient and abnormal lymph transport and, correspondingly, accumulation of protein-rich fluid in the interstitial space (tissue edema)[159,169,172]. Because the microvascular network is the principal site for fluid exchange between blood, lymph, and interstitial space, detailed studies of lymph microvessel disturbances during lymphedema have great importance. The efficacy of existing therapeutic treatments for PML is controversial, and clear scientific data have not emerged on the mechanisms of lymphedema development[143,170,171].

Obtaining data from human subjects involves many difficulties (e.g., unpredictability of the time of clinical

onset of PML, limitations of diagnostic methods, *etc.*)[170,173]. In experimental studies in rat, dog, and rabbit extremities, the multi-layers of lymph vascular networks, the rapid development of a good collateral network, and sufficient angiogenesis permit quick restoration of lymph pathways and drainage function, leading to prompt resolution of even acute edema without the appearance of long-term or chronic edema[174-177]. This precludes an informed study of chronic or long-term edema.

In light of these facts, the development of lymphedema in rat mesentery may make the detailed study of lymph and blood microvessel function in acute and chronic edema, because the single layer of vessels in this animal model reduces the opportunity for rapid development of collateral lymph flow. In our study, experimental lymphedema was created by microsurgical removal of regional lymph nodes (lymphadenectomy) or ligation of the collecting vein[101,126,178,179]. Then, the direct quantitative measurement of tissue water was performed in parallel to monitoring blood and lymph vessel activity, including mapping individual cell transport in microvessels and tissue.

After lymphadenectomy, dynamic observation of amounts of water revealed increasing edema from 30 min to 1 wk; the greatest degree of edema occurred at 1 wk with a gradual decrease in edema from 1 to 11 wk[101]. At the thirtieth minute post lymphadenectomy, these effects were accompanied by acute constriction of lymph vessels and slowing of lymph flow velocity from 302 ± 41 μm/s before extirpation to 155 ± 30 μm/s after extirpation ($P < 0.01$). After 1 wk of lymphedema, the lymphatics were overloaded (diameter increased from 133 ± 6 μm in their intact state to 147 ± 4 μm after lymphadenectomy, $P < 0.05$) with slowing lymph flow. Four weeks after lymphadenectomy, the amount of water in tissue included a range from significant compensation to progressive development of edema. In spite of this, lymph microvessels of all experimental animals (with compensation or with decompensation of edema) revealed significant dysfunction and structure damage (dilation, slowing of lymph flow, degenerative changes in the microlymphatic wall). Eleven weeks after lymphedema, we observed various microvascular disturbances, including lymphatic fibrosis at edema decompensation and significant dilation of lymph microvessels or lymphangiogenesis at edema compensation.

We obtained experimental evidence of the significant role of blood microvessels during lymphedema development after lymphadenectomy, which before was either not clear or was controversial. Marked changes in blood microvessels started at the stage of well-developed tissue edema and marked lymphatic disturbances. We observed dilation of blood microvessels, venules, and expansion of the microvascular network without significant hemorrhage in the interstitium[101].

Acute venous insufficiency (30 min after vein ligation) led to significant edema[101,126,178,179]. The comparison of acute lymphedema after lymphadenectomy and venous insufficiency revealed several similar changes, including inhibition of lymph flow and phasic activity. The specific disturbances after vein ligation included marked dilation of the blood vascular network; slowing (up to stasis) of blood flow in venules; and multiple hemorrhages adjacent to the venules and, as a result, the presence of many RBCs in the lymph.

Thus, unknown mechanisms of microvascular damage as well as the correlation between the functions of lymph microvessels, blood microvessels, and tissue edema in dynamic lymphedema development *in vivo* was established, which is important both for understanding mechanisms of lymphedema and for developing new treatment strategies.

Experimental model of sound-related stress

Experimental pathologic stress (2 h of immobilization and interrupted sound, 120 dB, 150-500 Hz) on rats led to significant (20%) increase in microlymphatic diameters ($P < 0.01$); intensification of lymph flow (mean cell velocity increased from 227 ± 8 μm/s in intact rats to 295 ± 12 μm/s in the stressed animals, $P < 0.001$), and stimulation of phasic contractions in 75% of lymphatics[179-181]. The resulting changes in lymph microvessel function probably stimulate lymph drainage and, therefore, play an adaptive role in this pathology.

REAL-TIME QUANTITATIVE MONITORING OF INDIVIDUAL CELL TRANSPORT *IN VIVO*

Normal rat lymphocytes, rat basophilic leukemia (RBL-1) cells, K562 human leukemia cells, and rat RBCs (for each cell type, 10^7-10^8 cells/mL) were labeled with FITC and introduced separately by bolus injection (100 μL) into the tail vein of rats with normal blood circulation or with acute venous insufficiency (ligation of collecting mesenteric vein). Over the next 30-60 min, we monitored in real-time the fluorescently labeled circulating, rolling, and adhesive cells in mesenteric blood vessels (diameter, 30-50 μm) and lymph microvessels (diameter, 120-180 μm), as well as visualized the distribution of the cells in mesenteric interstitial space. Simultaneous fluorescence and transmission imaging allowed us to distinguish the position of a single labeled cell. Accumulation of cells in mesenteric lymph nodes and the right lobe of the liver was monitored *in vivo* 60-90 min after the injections; each organ had been carefully exposed through a mid-abdominal incision and placed on a thermostabilizing microscope stage. To minimize light scattering by tissue and obtain deep, clear images of lymph nodes, we applied optical immersion technology (optical clearing method) using glycerol, which is an osmotic chemical[182,183]. In addition, the concentration of labeled cells in the systemic blood circulation was estimated by sampling blood through a catheter.

Normal and leukemic cell transport: a comparative analysis

We observed a significant number of rat RBCs, WBCs (lymphocytes), and leukemic cells in blood microvessels immediately after injection; 85%-95% of the cells were cleared from the microcirculation within the first 30 min (Figure 15A and B). In comparison, only a few human leukemia cells were found in the blood circulation within

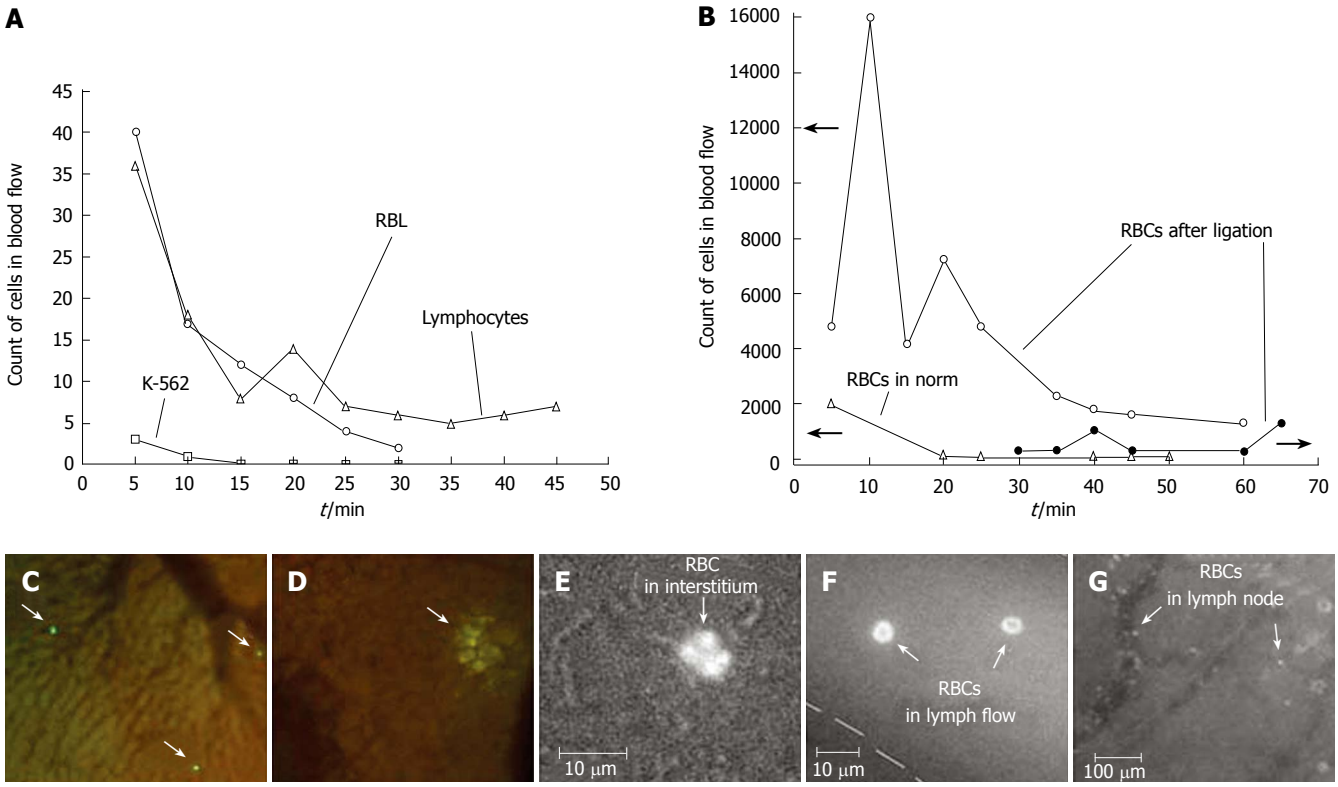

Figure 15 **A**: Monitoring of labeled rat lymphocytes, and rat (RBL) and human (K562) leukemia cells in blood vessels of rat mesentery; **B**: Simultaneous monitoring of RBCs in blood and lymph systems under normal conditions and with venous insufficiency; **C**, **D**: *In vivo* imaging of liver with (**C**) lymphocytes and (**D**) RBL leukemia cells. Monitoring RBC migration from blood vessel (**E**) through interstitium to (**F**) lymph vessel and (**G**) lymph node.

the first 5-10 min (Figure 15A), probably because 95% of the cells were cleared by a strong immune response immediately after injection. These cells then migrated into the interstitial space and were quickly destroyed. No cells appeared in lymphatic vessels during the first 60 min of observation.

In the first 5 min after bolus injections of WBCs or RBCs labeled with FITC (10^6 cells of each type in bolus), 50 times more RBCs were present in the circulation than were normal WBCs. Normal WBCs were detected in blood flow more often than rat leukemia cells (RBL-1 cells). RBL-1 cells, being ~1.5-2 times larger than normal WBCs, probably plugged small microvessels, thus decreasing the number of cells detected. In particular, Figure 15A shows that the number of WBCs was slightly higher than that of RBL-1 cells, although fewer WBCs (10^6 cells in bolus) than RBL-1 cells (10^7 cells in bolus) were injected. At 60-90 min of observation, both types of cells had accumulated mainly in the liver (Figure 15C and D). WBCs were visualized in liver as clearly distinguishable individual cells (Figure 15C), whereas RBL-1 cells appeared as a fluorescent spot (Figure 15D), probably because cells were destroyed in the liver, and only the rest of the dye was visible. However, both types of cells were identified after 3 h of observation in blood samples from large vessels; there were more WBCs than RBL-1 cells (10^3 *vs* 10^2). Thus, although the migrations of leukemic cells and normal cells in the same living organism represent some shared properties, they also display significantly distinct features. In the future, these distinct features may be used as diagnostic criteria for leukemia. Since the presented approach is able to analyze the transport of lymphocyte (important participants of immune response) it offers the potential to study *in vivo* immune responses at cellular and molecular levels.

Cell transport dynamic from blood to lymph during edema

The modeling of acute venous insufficiency and tissue edema caused marked changes in normal cell migration[101]. In particular, after injection of labeled RBCs, we observed a 5-min increase in the absolute number of labeled cells in the slowing blood flow of edematous tissue compared with normal blood flow (Figure 15B). Then, the slow-down of blood flow at the edema led to the output of many RBCs (10-15 min of observation) from blood vessels in mesenteric interstitium, where the trajectory of their motion is represented as episodic zigzag lines with mean velocities of 10-20 μm/s. As a result, RBCs moved through the interstitium to the lymphatics. After 30 min of monitoring, RBCs were identified in lymph flow (Figure 15F), and then in mesenteric lymph nodes (40-60 min of observation; Figure 15G). Thus, our integrated optical technique demonstrates unique capabilities for real-time monitoring of labeled cells in blood and lymph flow, as well as the migration of these cells into tissue interstitium and regional lymph nodes.

In vivo detection of flowing apoptotic cells

Apoptosis is referred to as programmed physiological cell death. *In vivo* study of apoptosis is crucial for understanding the fundamentals of cell biology; optimization of

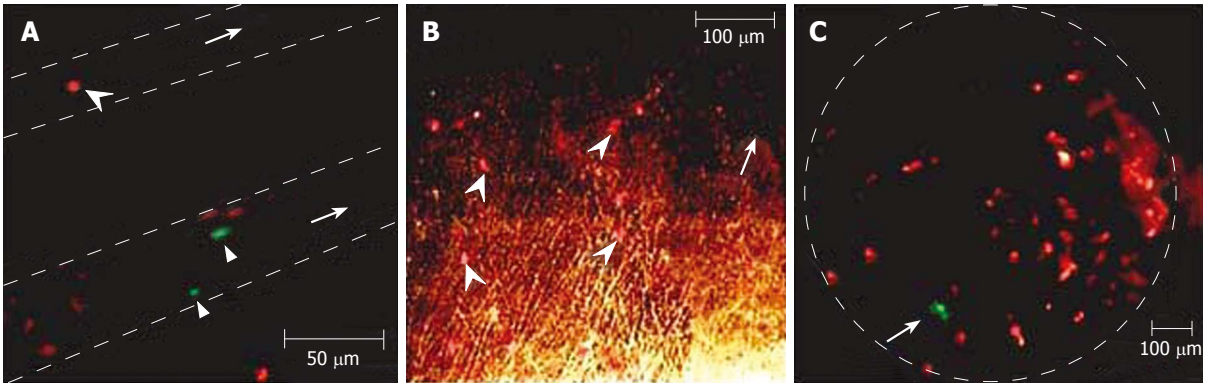

Figure 16 **A**: Apoptotic (arrowhead, red) and normal (two arrow triangles, green) cells in two blood vessels (dashed lines); **B**: Apoptotic cells (arrowhead, red) in interstitium (arrow shows one vessel); **C**: Normal (arrow, green) and apoptotic (red) cells in a lymph node (dashed line).

radiation therapy and chemotherapy; diagnosis of many diseases (e.g., metastasis development, cardiovascular diseases, hematological diseases, autoimmune diseases, neurodegenerative diseases, Alzheimer's disease); and assessment of acute organ transplant rejection or the effect of immunosuppressive drugs[134,184-195]. Despite significant progress in studying apoptosis *in vitro* with many powerful assays, adapting these assays to *in vivo* study of apoptosis is extremely difficult[184,185].

In our experiments, WBCs extracted from a rat underwent apoptosis after exposure to dexamethasone. They were then labeled with rhodamine 6G (red fluorescent emission). In addition, normal WBCs were labeled with FITC (green emission). A 50/50 mixture of labeled apoptotic and normal WBCs was injected into a rat's tail vein, and the appearance of the WBCs was monitored in rat mesentery venules with integrated PTFC. The fluorescence measurements (obtained by counting the number of cells in images) demonstrated the appearance of both normal and apoptotic cells in blood microvessel flow during the first minute (Figure 16A), and rapid clearing of apoptotic cells from circulation, with a half-life of ~8 min. We also observed: (1) rolling apoptotic cells in small venules within 10 min after the injections, (2) the appearance of apoptotic cells in the interstitium after 15 min (Figure 16B), and (3) significant accumulation of apoptotic cells in mesenteric lymph nodes (Figure 16C) after 30 min (see details of node location in Figure 3A and B).

Thus, the obtained results demonstrate that individual cell migration in living organisms depends on: (1) the morphological type of normal and abnormal cells (e.g. WBCs versus RBCs, WBCs versus leukemic cells), (2) the functional state of the cell (e.g. living versus apoptotic cells), and (3) the functional status of the entire organism (e.g. in norm versus in acute venous insufficiency at tissue edema). The high sensitivity of the PT technique to nanoscale morphologic events during apoptosis demonstrated *in vitro*[112-113], in combination with conventional fluorescent assays, makes it possible to apply this technique for detection of apoptotic cells *in vivo*.

IR ANGIOGRAPHY AND LYMPHGRAPHY

Indocianine green (ICG) is a well-known, relatively harmless dye for IR blood angiography and IR imaging of lymph nodes in human and animals[196-201]. Within the first seconds after intravenous injection, there is a shift in the absorption spectrum of ICG from 780 nm to 805 nm (spectral stabilization) due to two processes: polymerization of ICG molecules and their binding to plasma proteins and lipoproteins[196]. Plasma clearance of ICG is biphasic, showing a rapid first phase with a half-life of 4-6 min and a secondary phase with a half-life of more than 1 h[197]. ICG is eliminated from an organism by the enterohepatic route[197].

The imaging of blood vasculature by ICG is a well-known conventional approach; however, identification of the lymph microvascular network with ICG has not been previously studied. Recently, we performed first experiments with microlymphatics. Using TDM and fluorescent microscopy, we monitored typical microvascular units (venula, arteriola, and lymph microvessel of rat mesentery; Figure 17) after intravenous ICG injection (0.2 mL/100 g in rat's tail vein). Excitation at a wavelength of 805 nm, 0.25 mW/cm^2, was provided by continuous diode laser, and the re-emitted fluorescence was filtered at 830 nm and then detected using an intensified highly sensitive camera (PentoMAX, Roper Scientific). Our preliminary studies demonstrated that the first IR image of the venula appears 70-80 s after injection; then, in a short period of time (first 2 min after injection), dye appeared in the arteriola (Figure 17B). Forty to fifty minutes after injection, ICG accumulated (at least partly) in lymph microvessels (Figure 17C). Thus, ICG may potentially be used for study of blood and lymph microcirculation (IR angiography and lymphography), including a monitoring traffic dye in blood and lymph vascular nets.

CONCLUSIONS

As demonstrated in this paper, rat mesentery, in combination with advanced optical techniques, is an attractive animal model for *in vivo* lymph- and blood flow cytometry, high-resolution high speed cell imaging, IR time-resolved angiography and lymphography, real-time monitoring of cells traffic through tissue in norm, during diseases or in response to therapy.

Specifically, the capabilities of this model may include:

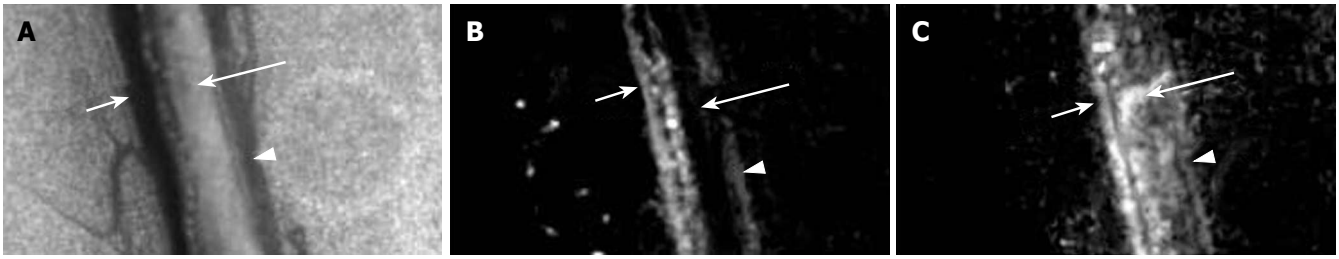

Figure 17 ICG IR blood and lymph microangiography. Transmission image before ICG injection (venula: short arrow, arteriola: triangle, lymph microvessel: long arrow) (**A**). Fluorescence images (excitation 805 nm; emission 830 nm) at the (**B**) 15th and (**C**) 45th min after ICG injection.

(1) analysis of cell pathways in tissue (blood microvessel, interstitium, afferent lymphatics) with migration through microvessel walls and accumulation in lymph nodes and liver; (2) quantitative monitoring of changes in the number of normal or abnormal cells in blood and lymph flow (blood and lymph FC); (3) identification of moving and static cells, including rare abnormal cells and apoptotic cells, through their size, shape, and specific sub-cellular structures; (4) high-resolution, high-speed monitoring of lymph and blood microrheology (e.g. transient deformability, cell aggregation), and interactions between different moving cells and between moving cells and endothelial cells of the vessel wall; (5) quantitative assessment of the clearance rate of circulating cells in lymph and blood flow; (6) analysis of *in vivo* immune responses at cellular and molecular levels; (7) *in vivo* monitoring of the circulation and migration of chylomicrons, bacteria, and viruses; (8) monitoring of dynamic thrombus and blood clot formation (with and without platelet participation); (9) label-free IR microvessel angiography and lymphography.

These advantages are crucial, both for understanding basic cell biology (e.g. metabolism and apoptosis), cell flow dynamics, and for conducting clinical studies of early disease diagnoses (e.g., cancer, sickle diseases, leukemia, edema, inflammation, infections) or assessment of innovative therapeutic interventions (pharmaceuticals, nicotine, lasers, or γ-radiation). Other potential applications may include radio and drug screening *in vivo* based on the previously described, promising *in vitro* techniques.

It is hoped that this review will serve not only as a helpful progress report and to provide certain leads for further research, but will also help attract the scientific interest and support that are required to solve these problems.

ACKNOWLEDGMENTS

The authors thank Grigory E Brill, PhD, DSc (Saratov Medical State University, Russia); Sergey S Ulianov, PhD, DSc (Saratov State University, Russia); Qingming Luo, PhD (Institute for Biomedical Photonics, Huazhong University of Science and Technology, China); Ivan V Fedosov, PhD (Saratov State University, Russia); Anastasia V Solovieva, PhD (Saratov Medical State University, Russia). We thank Tatiana V Stepanova for assisting with animal experiments, Dmitri O Lapotko, PhD for his significant contribution in the development of the PT setup, and Scott Ferguson, for assisting with laser measurements. We also thank the Office of Grants and Scientific Publications at the University of Arkansas for Medical Sciences for editorial assistance during the preparation of this manuscript.

REFERENCES

1 **Aukland K**. Arnold Heller and the lymph pump. *Acta Physiol Scand* 2005; **185**: 171-180
2 **Zweifach BW**, Lowenstein B, Chambers R. Response of blood capillaries to acute hemorrhage in the rat. *Am J Physiol* 1944; **142**: 80-93
3 **Chambers R**, Zweifach BW. Topography and function of the mesenteric capillary circulation. *Am J Anat* 1944; **75**: 173-205
4 **Wiggers CJ**. Peripheral circulation. *Annu Rev Physiol* 1947; **9**: 255-300
5 **Gaehtgens P**, Meiselman HJ, Wayland H. Erythrocyte flow velocities in mesenteric microvessels of the cat. *Microvasc Res* 1970; **2**: 151-162
6 **Johnson PC**. Red cell separation in the mesenteric capillary network. *Am J Physiol* 1971; **221**: 99-104
7 **Zweifach BW**, Prather JW. Micromanipulation of pressure in terminal lymphatics in the mesentery. *Am J Physiol* 1975; **228**: 1326-1335
8 **Starr MC**, Frasher WG. In vivo cellular and plasma velocities in microvessels of the cat mesentery. *Microvasc Res* 1975; **10**: 102-106
9 **Lipowsky HH**, Usami S, Chien S. In vivo measurements of "apparent viscosity" and microvessel hematocrit in the mesentery of the cat. *Microvasc Res* 1980; **19**: 297-319
10 **Firrell JC**, Lipowsky HH. Leukocyte margination and deformation in mesenteric venules of rat. *Am J Physiol* 1989; **256**: H1667-H1674
11 **Seki J**. Flow pulsation and network structure in mesenteric microvasculature of rats. *Am J Physiol* 1994; **266**: H811-H821
12 **Yamaki K**, Lindbom L, Thorlacius H, Hedqvist P, Raud J. An approach for studies of mediator-induced leukocyte rolling in the undisturbed microcirculation of the rat mesentery. *Br J Pharmacol* 1998; **123**: 381-389
13 **Frenette PS**, Moyna C, Hartwell DW, Lowe JB, Hynes RO, Wagner DD. Platelet-endothelial interactions in inflamed mesenteric venules. *Blood* 1998; **91**: 1318-1324
14 **Jiang Y**, Liu AH, Zhao KS. Studies on the flow and distribution of leukocytes in mesentery microcirculation of rats. *World J Gastroenterol* 1999; **5**: 231-234
15 **Pearson MJ**, Lipowsky HH. Influence of erythrocyte aggregation on leukocyte margination in postcapillary venules of rat mesentery. *Am J Physiol Heart Circ Physiol* 2000; **279**: H1460-H1471
16 **Osterloh K**, Gaehtgens P, Pries AR. Determination of microvascular flow pattern formation in vivo. *Am J Physiol Heart Circ Physiol* 2000; **278**: H1142-H1152
17 **He P**, Wang J, Zeng M. Leukocyte adhesion and microves-

sel permeability. *Am J Physiol Heart Circ Physiol* 2000; **278**: H1686-H1694
18 **Sugii Y**, Nishio S, Okamoto K. In vivo PIV measurement of red blood cell velocity field in microvessels considering mesentery motion. *Physiol Meas* 2002; **23**: 403-416
19 **Sugii Y**, Nishio S, Okamoto K. Measurement of a velocity field in microvessels using a high resolution PIV technique. *Ann N Y Acad Sci* 2002; **972**: 331-336
20 **Golub AS**, Pittman RN. Erythrocyte-associated transients in PO2 revealed in capillaries of rat mesentery. *Am J Physiol Heart Circ Physiol* 2005; **288**: H2735-H2743
21 **Ohshima N**. Engineering approaches to the microcirculation studies. *Clin Hemorheol Microcirc* 2006; **34**: 27-34
22 **Benoit JN**, Zawieja DC, Goodman AH, Granger HJ. Characterization of intact mesenteric lymphatic pump and its responsiveness to acute edemagenic stress. *Am J Physiol* 1989; **257**: H2059-H2069
23 **Benoit JN**. Relationships between lymphatic pump flow and total lymph flow in the small intestine. *Am J Physiol* 1991; **261**: H1970-H1978
24 **Sekizuka E**, Ohshio C, Minamitani H. Automatic analysis of moving images for the lymphocyte velocity measurement. *Microcirculation annual* 1995; **11**: 107-108
25 **Takahashi T**, Shibata M, Kamiya A. Mechanism of macromolecule concentration in collecting lymphatics in rat mesentery. *Microvasc Res* 1997; **54**: 193-205
26 **Dixon JB**, Zawieja DC, Gashev AA, Coté GL. Measuring microlymphatic flow using fast video microscopy. *J Biomed Opt* 2005; **10**: 064016
27 **Zweifach BW**, Kivy-Rosenberg E. Microcirculatory effects of whole-body X-irradiation and radiomimetic procedures. *Am J Physiol* 1965; **208**: 492-498
28 **Ferguson MK**, Shahinian HK, Michelassi F. Lymphatic smooth muscle responses to leukotrienes, histamine and platelet activating factor. *J Surg Res* 1988; **44**: 172-177
29 **Aukland K**, Reed RK. Interstitial-lymphatic mechanisms in the control of extracellular fluid volume. *Physiol Rev* 1993; **73**: 1-78
30 **Benoit JN**. Effects of alpha-adrenergic stimuli on mesenteric collecting lymphatics in the rat. *Am J Physiol* 1997; **273**: R331-R336
31 **Kimura M**, Mitani H, Bandoh T, Totsuka T, Hayashi S. Mast cell degranulation in rat mesenteric venule: effects of L-NAME, methylene blue and ketotifen. *Pharmacol Res* 1999; **39**: 397-402
32 **Carati CJ**, **Jobling J**, Fouyaxis J and **Gannon BJ.** Effect of low level laser on mesenteric lymphatics and blood vessels in-vivo. *Progress in Microcirculation Research* 1999; **10**: 77-80
33 **Torres LN**, Torres Filho IP. Determination of macromolecular exchange and PO2 in the microcirculation: a simple system for in vivo fluorescence and phosphorescence videomicroscopy. *Braz J Med Biol Res* 2001; **34**: 129-135
34 **Amerini S**, Ziche M, Greiner ST, Zawieja DC. Effects of substance P on mesenteric lymphatic contractility in the rat. *Lymphat Res Biol* 2004; **2**: 2-10
35 **Shirasawa Y**, Ikomi F, Ohhashi T. Physiological roles of endogenous nitric oxide in lymphatic pump activity of rat mesentery in vivo. *Am J Physiol Gastrointest Liver Physiol* 2000; **278**: G551-G556
36 **Arshi K**, Bendayan M, Ghitescu LD. Alterations of the rat mesentery vasculature in experimental diabetes. *Lab Invest* 2000; **80**: 1171-1184
37 **Yanagi K**, Ohshima N. Angiogenic vascular growth in the rat peritoneal disseminated tumor model. *Microvasc Res* 1996; **51**: 15-28
38 **Hayes H**, Kossmann E, Wilson E, Meininger C, Zawieja D. Development and characterization of endothelial cells from rat microlymphatics. *Lymphat Res Biol* 2003; **1**: 101-119
39 **Ji RC**. Characteristics of lymphatic endothelial cells in physiological and pathological conditions. *Histol Histopathol* 2005; **20**: 155-175
40 **Witte MH**, Jones K, Wilting J, Dictor M, Selg M, McHale N, Gershenwald JE, Jackson DG. Structure function relationships in the lymphatic system and implications for cancer biology. *Cancer Metastasis Rev* 2006; **25**: 159-184
41 **Morisaki H**, Katayama T, Kotake Y, Ito M, Handa M, Ikeda Y, Takeda J, Suematsu M. Carbon monoxide modulates endotoxin-induced microvascular leukocyte adhesion through platelet-dependent mechanisms. *Anesthesiology* 2002; **97**: 701-709
42 **Mouthon MA**, Vereycken-Holler V, Van der Meeren A, Gaugler MH. Irradiation increases the interactions of platelets with the endothelium in vivo: analysis by intravital microscopy. *Radiat Res* 2003; **160**: 593-599
43 **Yamagata K**, Kumagai K. Experimental study of lymphogenous peritoneal cancer dissemination: migration of fluorescent-labelled tumor cells in a rat model of mesenteric lymph vessel obstruction. *J Exp Clin Cancer Res* 2000; **19**: 211-217
44 **Bornhop DJ**, Contag CH, Licha K, Murphy CJ. Advance in contrast agents, reporters, and detection. *J Biomed Opt* 2001; **6**: 106-110
45 **Contag PR**, Olomu IN, Stevenson DK, Contag CH. Bioluminescent indicators in living mammals. *Nat Med* 1998; **4**: 245-247
46 **Ebert B**, Sukowski U, Grosenick D, Wabnitz H, Moesta KT, Licha K, Becker A, Semmler W, Schlag PM, Rinneberg H. Near-infrared fluorescent dyes for enhanced contrast in optical mammography: phantom experiments. *J Biomed Opt* 2001; **6**: 134-140
47 **Becker MD**, Planck SR, Crespo S, Garman K, Fleischman RJ, Dullforce P, Seitz GW, Martin TM, Parker DC, Rosenbaum JT. Immunohistology of antigen-presenting cells in vivo: a novel method for serial observation of fluorescently labeled cells. *Invest Ophthalmol Vis Sci* 2003; **44**: 2004-2009
48 **Nestmann ER**, Douglas GR, Matula TI, Grant CE, Kowbel DJ. Mutagenic activity of rhodamine dyes and their impurities as detected by mutation induction in Salmonella and DNA damage in Chinese hamster ovary cells. *Cancer Res* 1979; **39**: 4412-4417
49 **Saetzler RK**, Jallo J, Lehr HA, Philips CM, Vasthare U, Arfors KE, Tuma RF. Intravital fluorescence microscopy: impact of light-induced phototoxicity on adhesion of fluorescently labeled leukocytes. *J Histochem Cytochem* 1997; **45**: 505-513
50 **Zdolsek JM**. Acridine orange-mediated photodamage to cultured cells. *APMIS* 1993; **101**: 127-132
51 **Abbitt KB**, Rainger GE, Nash GB. Effects of fluorescent dyes on selectin and integrin-mediated stages of adhesion and migration of flowing leukocytes. *J Immunol Methods* 2000; **239**: 109-119
52 **Berk DA**, Swartz MA, Leu AJ, Jain RK. Transport in lymphatic capillaries. II. Microscopic velocity measurement with fluorescence photobleaching. *Am J Physiol* 1996; **270**: H330-H337
53 **Novak J**, Georgakoudi I, Wei X, Prossin A, Lin CP. In vivo flow cytometer for real-time detection and quantification of circulating cells. *Opt Lett* 2004; **29**: 77-79
54 **Georgakoudi I**, Solban N, Novak J, Rice WL, Wei X, Hasan T, Lin CP. In vivo flow cytometry: a new method for enumerating circulating cancer cells. *Cancer Res* 2004; **64**: 5044-5047
55 **Wei X**, Sipkins DA, Pitsillides CM, Novak J, Georgakoudi I, Lin CP. Real-time detection of circulating apoptotic cells by in vivo flow cytometry. *Mol Imaging* 2005; **4**: 415-416
56 **Pries AR**, Eriksson SE, Jepsen H. Real-time oriented image analysis in microcirculatory research. *Proc SPIE* 1989; **1357**: 257-263
57 **Skalak R**, Branemark PI. Deformation of red blood cells in capillaries. *Science* 1969; **164**: 717-719
58 **Galanzha EI**, Tuchin VV, Zharov VP. In vivo integrated flow image cytometry and lymph/blood vessels dynamic microscopy. *J Biomed Opt* 2005; **10**: 054018
59 **Kim S**, Popel AS, Intaglietta M, Johnson PC. Aggregate formation of erythrocytes in postcapillary venules. *Am J Physiol Heart Circ Physiol* 2005; **288**: H584-H590
60 **Rusznyak I**, Foldi M, Szabo G. Lymphatics and Lymph Circulation. 2nd ed. London: Pergamon, 1967
61 **Human Physiology**, Schmidt RF, Thews G, editors. Berlin

Heidelberg: Springer-Verlag, 1989
62 **Brown P**. Lymphatic system: unlocking the drains. *Nature* 2005; **436**: 456-458
63 **Schmid-Schönbein GW**. Microlymphatics and lymph flow. *Physiol Rev* 1990; **70**: 987-1028
64 **McHale NG**. Role of the lymph pump and its control. *NIPS* 1995; **10**: 112-117
65 **Vajda J**, Tomcsik M. The structure of the valves of the lymphatic vessels. *Acta Anat* (Basel) 1971; **78**: 521-531
66 **Galanzha EI**, Brill GE, Aizu Y, Ulyanov SS, Tuchin VV. Speckle and Doppler Methods of Blood and Lymph Flow Monitoring. In: Handbook of Optical Biomedical Diagnostics, Bellingham: SPIE Press, 2002: 875-937
67 **Galanzha EI**, Tuchin VV, Zharov VP, Solovieva AV, Stepanova TV, Brill GE. The diagnosis of lymph microcirculation on rat mesentery in vivo. *Proc SPIE* 2003; **4965**: 325- 333
68 **Galanzha EI**, Ulyanov SS, Tuchin VV, Brill GE, Solov`eva AV, Sedykh AV. Comparison of lymph and blood flow in microvessels: coherent optical measurements. *Proc SPIE* 2000; **4163**: 94-98
69 **Johnston MG**. The intrinsic lymph pump: progress and problems. *Lymphology* 1989; **22**: 116-122
70 **Mordon S**, Begu S, Buys B, Tourne-Peteilh C, Devoisselle JM. Study of platelet behavior in vivo after endothelial stimulation with laser irradiation using fluorescence intravital videomicroscopy and PEGylated liposome staining. *Microvasc Res* 2002; **64**: 316-325
71 **Baez S**. An open cremaster muscle preparation for the study of blood vessels by in vivo microscopy. *Microvasc Res* 1973; **5**: 384-394
72 **Haier J**, Korb T, Hotz B, Spiegel HU, Senninger N. An intravital model to monitor steps of metastatic tumor cell adhesion within the hepatic microcirculation. *J Gastrointest Surg* 2003; **7**: 507-514; discussion 514-515
73 **Schacht V**, Berens von Rautenfeld D, Abels C. The lymphatic system in the dorsal skinfold chamber of the Syrian golden hamster in vivo. *Arch Dermatol Res* 2004; **295**: 542-548
74 **Vargas G**, Readinger A, Dozier SS, Welch AJ. Morphological changes in blood vessels produced by hyperosmotic agents and measured by optical coherence tomography. *Photochem Photobiol* 2003; **77**: 541-549
75 **Galanzha EI**, Tuchin VV, Solov`eva AV, Stepanova TV, Luo Q, Cheng H. Skin backreflectance and microvascular system functioning at the action of osmotic agents. *J Phys D: Appl Phys* 2003; **36**: 1-8
76 **Zharov V**, Galanzha E, Shashkov E, Khlebtsov N, Tuchin V. *In vivo* photoacoustic flow cytometry for real-time monitoring of circulating cells and nanoparticles. *SPIE News room* 2006
77 **Zharov V**, Galanzha E, Shashkov E, Khlebtsov N, Tuchin V. *In vivo* integrated photoacoustic flow cytometry: Application for monitoring circulating cancer cells labeled with gold nanorods. Fifth Workshop on Optical Imaging from Bench to Bedside at the national Institutes of Health 2006: 126
78 **Kalchenko V**, Plaks V. Intravital Video Microscopy – From Simple Solutions to a Multiuser Core Facility. *Proc RMS* 2005; **40**: 221-226
79 **Kersey TW**, Van Eyk J, Lannin DR, Chua AN, Tafra L. Comparison of intradermal and subcutaneous injections in lymphatic mapping. *J Surg Res* 2001; **96**: 255-259
80 **Hirsch JI**, Tisnado J, Cho SR, Beachley MC. Use of isosulfan blue for identification of lymphatic vessels: experimental and clinical evaluation. *AJR Am J Roentgenol* 1982; **139**: 1061-1064
81 **Bowen CH**, Albertine KH. Initial lymphatics are present in the loose areolar connective tissue of the golden hamster's cheek pouch. *Microvasc Res* 1988; **35**: 236-241
82 **Schwerte T**, Pelster B. Digital motion analysis as a tool for analysing the shape and performance of the circulatory system in transparent animals. *J Exp Biol* 2000; **203**: 1659-1669
83 **Yaniv K**, Isogai S, Castranova D, Dye L, Hitomi J, Weinstein BM. Live imaging of lymphatic development in the zebrafish. *Nat Med* 2006; **12**: 711-716
84 **Weinstein B**. Vascular cell biology in vivo: a new piscine paradigm? *Trends Cell Biol* 2002; **12**: 439-445
85 **Baker HJ**, Lindsey JR, Weisbroth SH. The Laboratory Rat. New York: Academic, 1979
86 **Gill TJ**. The rat in biomedical research. *Physiologist* 1985; **28**: 9-17
87 **Gill TJ**, Smith GJ, Wissler RW, Kunz HW. The rat as an experimental animal. *Science* 1989; **245**: 269-276
88 **Murakami T**, Kobayashi E. Color-engineered rats and luminescent LacZ imaging: a new platform to visualize biological processes. *J Biomed Opt* 2005; **10**: 41204
89 **Gahm T**, Witte S. Measurement of the optical thickness of transparent tissue layers. *J Microsc* 1986; **141**: 101-110
90 **Barber BJ**, Oppenheimer J, Zawieja DC, Zimmermann HA. Variations in rat mesenteric tissue thickness due to microvasculature. *Am J Physiol* 1987; **253**: G549-G556
91 **Ghassemifar R**, Franzén L. A double-embedding technique for thin tissue membranes. *Biotech Histochem* 1992; **67**: 363-366
92 **Physiology of Blood Circulation: Physiology of vascular system**. Tkachenko BI, editor. Leningrad: Nauka, 1984 (in Russian)
93 **Chernuh AM**, Alexandrov PN, Alexeev OV. Microcirculation. Moscow: Medicine, 1984 (in Russian)
94 **Zharov VP**, Galanzha EI, Tuchin VV. In vivo photothermal flow cytometry: imaging and detection of individual cells in blood and lymph flow. *J Cell Biochem* 2006; **97**: 916-932
95 **Hauck G**. Functional aspects of the topical relationship between blood capillaries and lymphatics of the mesentery. *Pflugers Arch* 1973; **339**: 251-256
96 **Hauck G**. Origin of the mesenteric lymphatics and their topical relationship to the blood capillaries. *Bibl Anat* 1973; **12**: 356-360
97 **Tuchin VV**. The lasers and fiber optic in biomedical research. Saratov: Saratov State University Press, 1998 (In Russian)
98 **Galanzha EI**, Tuchin VV, Ulyanov SS, Solov'eva AV, Luo Q, Cheng H. Optical properties of lymph flow in single microvessels: biomicroscopic, speckle-interferometric, and spectroscopic measurements. *Proc SPIE* 2001; **4434**: 197-203
99 **Scheinecker C**. Application of in vivo microscopy: evaluating the immune response in living animals. *Arthritis Res Ther* 2005; **7**: 246-252
100 **Horstick G**, Kempf T, Lauterbach M, Ossendorf M, Kopacz L, Heimann A, Lehr HA, Bhakdi S, Meyer J, Kempski O. Plastic foil technique attenuates inflammation in mesenteric intravital microscopy. *J Surg Res* 2000; **94**: 28-34
101 **Galanzha EI**, Tuchin VV, Zharov VP. Optical monitoring of microlympatic disturbances during experimental lymphedema, *Lymphat Res Biol*, 2007: In press
102 **Givan AL**. Principles of flow cytometry: an overview. *Methods Cell Biol* 2001; **63**: 19-50
103 **Chung A**, Karlan S, Lindsley E, Wachsmann-Hogiu S, Farkas DL. In vivo cytometry: a spectrum of possibilities. *Cytometry A* 2006; **69**: 142-146
104 **Zharov VP**, Galanzha EI, Menyaev Y, Tuchin VV. In vivo high-speed imaging of individual cells in fast blood flow. *J Biomed Opt* 2006; **11**: 054034
105 **Zharov VP**, Letokhov VS. Laser Optoacoustic Spectroscopy. Berlin Heidelberg, New York: Springer-Verlag, 1986
106 **Zharov VP**. Laser optoacoustic spectroscopy in chromatography. In: Laser Analytical Spectrochemistry. Letokhov VS, editor. Boston, Mass: Bristol, 1986: 229-271
107 **Lapotko D**, Kuchinsky G, Potapnev M, Pechkovsky D. Photothermal image cytometry of human neutrophils. *Cytometry* 1996; **24**: 198-203
108 **Lapotko D**, Romanovskaya T, Kutchinsky G, Zharov V. Photothermal studies of modulating effect of photoactivated chlorin on interaction of blood cells with bacteria. *Cytometry* 1999; **37**: 320-326
109 **Zharov VP** and Lapotko DO. Photothermal imaging of nanoparticles and cells (review). *IEEE J Sel Topics Quant Electron* 2005; **11**: 733-751
110 **Tokeshi M**, Uchida M, Hibara A, Sawada T, Kitamori T. Determination of subyoctomole amounts of nonfluorescent

molecules using a thermal lens microscope: subsingle-molecule determination. *Anal Chem* 2001; **73**: 2112-2116
111 **Tamaki E**, Sato K, Tokeshi M, Sato K, Aihara M, Kitamori T. Single-cell analysis by a scanning thermal lens microscope with a microchip: direct monitoring of cytochrome c distribution during apoptosis process. *Anal Chem* 2002; **74**: 1560-1564
112 **Zharov VP**, Galitovsky V, Chowdhury P. Nanocluster model of photothermal assay: application for high-sensitive monitoring of nicotine-induced changes in metabolism, apoptosis, and necrosis at a cellular level. *J Biomed Opt* 2005; **10**: 44011
113 **Zharov VP**, Galitovskiy V, Lyle CS, Chambers TC. Superhigh-sensitivity photothermal monitoring of individual cell response to antitumor drug. *J Biomed Opt* 2006; 11: 064034
114 **Zharov VP**, Galanzha EI, Shashkov EV, Khlebtsov NG, Tuchin VV. In vivo photoacoustic flow cytometry for monitoring of circulating single cancer cells and contrast agents. *Opt Lett* 2006; **31:** 3623-3625
115 **Zharov VP**, Galanzha EI, Tuchin VV. Photothermal image flow cytometry in vivo. *Opt Lett* 2005; **30**: 628-630
116 **Zharov VP**, Galanzha EI, Tuchin VV. Integrated photothermal flow cytometry in vivo. *J Biomed Opt* 2005; **10**: 051502
117 **Zharov VP**, Galanzha EI, Tuchin VV. Confocal photothermal flow cytometry in vivo. *Proc SPIE* 2005; **5697**: 167-176
118 **Zharov V**, Menyaev Y, Shashkov E, Galanzha E, Khlebtsov B, Scheludko A, Zimnyakov D, and Tuchin V. Fluctuation of probe beam in thermolens schematics as potential indicator of cell metabolism, apoptosis, necrosis and laser impact. *Proc SPIE* 2006; **6085**: 10-21
119 **Bednov AA**, Ul'yanov SS, Tuchin VV, Brill GE, Zakharova (Galanzha) EI. Investigation of lymph dynamics by speckle-interferometry method. *Applied Nonlinear Dynamics* 1996; **4**: 45-54
120 **Bednov AA**, Brill GE, Tuchin VV, Ul`yanov SS, Zakharova (Galanzha) EI. Blood flow measurements in microvessels using focused laser beam diffraction phenomenon. *Proc SPIE* 1994; **2370**: 379-383
121 **Starukhin P**, Ulyanov S, Galanzha E, Tuchin V. Blood-flow measurements with a small number of scattering events. *Appl Opt* 2000; **39**: 2823-2830
122 **Ul`yanov SS**, Tuchin VV, Bednov AA, Zakharova (Galanzha) EI, Brill GE. The application of Speckle Interferometry for the Monitoring of Blood and Lymph Flow in Microvessels. *Lasers in Med Sci* 1997; **12**: 31-41
123 **Fedosov IV**, Ulianov SS, Galanzha EI, Galanzha VA, Tuchin VV. Laser Doppler and Speckle techniques for bioflow measurements. In: Handbook of Coherent Domain Optical Methods. *Springer*, 2004; XLII, **1**: 397-437
124 **Fedosov IV**, Tuchin VV, Galanzha EI, Solov'eva AV, Stepanova TV. Recording of lymph flow dynamics in microvessels using correlation properties of scattered coherent radiation. *Quantum Electronics* 2002; **32**: 970-974
125 **Brill' GE**, Galanzha EI, Ul'ianov SS, Tuchin VV, Stepanova TV, Solov'eva AV. [Functional organization of lymphatic microvessels of the rat mesentery]. *Ross Fiziol Zh Im I M Sechenova* 2001; **87**: 600-607
126 **Galanzha EI**, Tuchin VV, Solovieva AV, Zharov VP. Experimental evaluation on the transmission optical microscopy for the diagnosis of lymphedema. J Xray Sci Technol 2002; **10**: 215-223
127 **Smith JB**, McIntosh GH, Morris B. The traffic of cells through tissues: a study of peripheral lymph in sheep. *J Anat* 1970; **107**: 87-100
128 **Ikomi F**, Hunt J, Hanna G, Schmid-Schönbein GW. Interstitial fluid, plasma protein, colloid, and leukocyte uptake into initial lymphatics. *J Appl Physiol(1985)* 1996; **81**: 2060-2067
129 **Young AJ**. The physiology of lymphocyte migration through the single lymph node in vivo. *Semin Immunol* 1999; **11**: 73-83
130 **Hall JG**, Morris B. The origin of the cells in the efferent lymph from a single lymph node. *J Exp Med* 1965; **121**: 901-910
131 **Dixon JB**, Greiner ST, Gashev AA, Cote GL, Moore JE, Zawieja DC. Lymph flow, shear stress, and lymphocyte velocity in rat mesenteric prenodal lymphatics. *Microcirculation* 2006; **13**: 597-610
132 **Azzali G**. On the transendothelial passage of tumor cell from extravasal matrix into the lumen of absorbing lymphatic vessel. *Microvasc Res* 2006; **72**: 74-85
133 **Zharov V**, Galanzha E and Tuchin V. Photothermal imaging of moving cells in lymph and blood flow in vivo. *Proc SPIE* 2004; **5320**: 256-263
134 **Gourley PL**, Hendricks JK, McDonald AE, Copeland RG, Barrett KE, Gourley CR, Singh KK, Naviaux RK. Mitochondrial correlation microscopy and nanolaser spectroscopy - new tools for biophotonic detection of cancer in single cells. *Technol Cancer Res Treat* 2005; **4**: 585-592
135 **Gourley PL**, Hendricks JK, McDonald AE, Copeland RG, Barrett KE, Gourley CR, Naviaux RK. Ultrafast nanolaser flow device for detecting cancer in single cells. *Biomed Microdevices* 2005; **7**: 331-339
136 **Brill GE**, Tuchin VV, Zakharova (Galanzha) EI, Ul`yanov SS. Influence of low power laser irradiation on lymph microcirculation at the increasing of NO production. *Proc SPIE* 1999; **3726**: 157-162
137 **Galanzha EI**, Brill' GE, Solov'eva AV, Stepanova TV. [Nitric oxide in the lymphatic microvessel regulation]. *Ross Fiziol Zh Im I M Sechenova* 2002; **88**: 983-989
138 **Pitts LH**, Young AR, McCulloch J, MacKenzie E. Vasomotor effects of dimethyl sulfoxide on cat cerebral arteries in vitro and in vivo. *Stroke* 1986; **17**: 483-487
139 **Jacob SW**, Herschler R. Pharmacology of DMSO. *Cryobiology* 1986; **23**: 14-27
140 **Lockie LM**, Norcross BM. A clinical study on the effects of dimethyl sulfoxide in 103 patients with acute and chronic musculoskeletal injuries and inflammations. *Ann N Y Acad Sci* 1967; **141**: 599-602
141 **Spruance SL**, McKeough MB, Cardinal JR. Dimethyl sulfoxide as a vehicle for topical antiviral chemotherapy. *Ann N Y Acad Sci* 1983; **411**: 28-33
142 **Brill' GE**, Zakharova EI. [The effect of dimethyl sulfoxide on the changes in the lymph microcirculation induced by staphylococcal toxin]. *Eksp Klin Farmakol* 1998; **61**: 54-56
143 **Piller NB**, Thelander A. Treatment of chronic postmastectomy lymphedema with low level laser therapy: a 2.5 year follow-up. *Lymphology* 1998; **31**: 74-86
144 **Carati CJ**, Anderson SN, Gannon BJ, Piller NB. Treatment of postmastectomy lymphedema with low-level laser therapy: a double blind, placebo-controlled trial. *Cancer* 2003; **98**: 1114-1122
145 **Kaviani A**, Yousefi R, Mortaz HS and Ghodsi M. Postmastectomy lymphedema; application of low-level laser therapy. *Laser Sur Med* 2003; **S15**: 66-68
146 **Brill GE**, Zakharova (Galanzha) EI. Influence of low power laser radiation on lymphatic microvessels. Abstract book of the 5th Congress of the Asian-Pacific Association for Laser Medicine and Surgery; 1994 Nov. 20-25; Tel Aviv, Israel. Israel, 1994: 17
147 **Verkruysse W**, Beek JF, VanBavel E, van Gemert MJ, Spaan JA. Laser pulse impact on rat mesenteric blood vessels in relation to laser treatment of port wine stain. *Lasers Surg Med* 2001; **28**: 461-468
148 **Zharov VP**, Galitovsky V and Viegas M. Photothermal detection of local thermal effects during selective nanophotothermolysis. *Appl Phys Lett* 2003; **83**: 4897-4899
149 **Zharov VP**, Galitovskaya EN, Johnson C, Kelly T. Synergistic enhancement of selective nanophotothermolysis with gold nanoclusters: potential for cancer therapy. *Lasers Surg Med* 2005; **37**: 219-226
150 **Zharov VP**, Letfullin RR, and Galitovskaya EN. Microbubbles-overlapping mode for laser killing of cancer cells with absorbing nanoparticle clusters. *J Physics D: Appl Phys* 2005; **38**: 2571-2581
151 **Zharov VP**, Kim JW,Curiel DT, Everts M. Self-assembling nanoclusters in living systems: application for integrated

photothermal nanodiagnostics and nanotherapy. *J Nanomedicine* 2005; **1**: 326-345
152 **Zharov VP**, Mercer KE, Galitovskaya EN, Smeltzer MS. Photothermal nanotherapeutics and nanodiagnostics for selective killing of bacteria targeted with gold nanoparticles. *Biophys J* 2006; **90**: 619-627
153 **Everts M**, Saini V, Leddon JL, Kok RJ, Stoff-Khalili M, Preuss MA, Millican CL, Perkins G, Brown JM, Bagaria H, Nikles DE, Johnson DT, Zharov VP, Curiel DT. Covalently linked Au nanoparticles to a viral vector: potential for combined photothermal and gene cancer therapy. *Nano Lett* 2006; **6**: 587-591
154 **Saini V**, Zharov VP, Brazel CS, Nikles DE, Johnson DT, Everts M. Combination of viral biology and nanotechnology: new applications in nanomedicine. *Nanomedicine* 2006; **2**: 200-206
155 **Chowdhury P**, MacLeod S, Udupa KB, Rayford PL. Pathophysiological effects of nicotine on the pancreas: an update. *Exp Biol Med* (Maywood) 2002; **227**: 445-454
156 **A report of Surgeon General: The Health Consequences of Smoking**. Department of Health & Human Services, Public Health Services, Centers for Disease Control & Prevention, National Center for chronic disease prevention and health promotion, office of smoking & health, Washington, D.C. 2004
157 **Armitage AK**, Dollery CT, George CF, Houseman TH, Lewis PJ, Turner DM. Absorption and metabolism of nicotine from cigarettes. *Br Med J* 1975; **4**: 313-316
158 **Galanzha EL**, Chowhury P, Tuchim VV, Zharov VP. Monitoring of nicotine impact in microlymphatics of rat mesentery with time-resolved microscopy. *Lymphology* 2005; **38**: 181-192
159 **Jeltsch M**, Tammela T, Alitalo K, Wilting J. Genesis and pathogenesis of lymphatic vessels. *Cell Tissue Res* 2003; **314**: 69-84
160 **Arbuthnott JP**. Staphylococcal α-toxin. In: Microbiological toxins. New York, 1970: 189-236
161 **Brown DA**. Some effects of staphylococcal alpha-toxin on the cardiovascular system. *Br J Pharmacol Chemother* 1966; **26**: 580-590
162 **Thelestam M**, Blomqvist L. Staphylococcal alpha toxin--recent advances. *Toxicon* 1988; **26**: 55-65
163 **Brill GE**, Sergeev IP, Glazkova EI, Morokhovets NV. [Effect of staphylococcal toxin on the microcirculatory system]. *Patol Fiziol Eksp Ter* 1992; (**1**): 21-23
164 **Brill GE**, Zakharova (Galanzha) EI. The lymphatic microvessels disfunction under the influence of staphylococcal toxin. Proceedings of the 6th World Congress for Microcirculation; 1996 Aug 25-30; Munich, Germany. Messmer K, Kubler WM, editors. International Proceedings Division: Monduzzi Editore, 1996: 179-182
165 **Brill GE**, Zakharova (Galanzha) EI. Pharmacological correction of lymph microcirculation disorders induced by staphylococcal toxin. Proceedings of the 6th World Congress for Microcirculation; 1996 Aug 25-30; Munich, Germany. Messmer K, Kubler WM, editors. International Proceedings Division: Monduzzi Editore, 1996: 175-177
166 **Brill GE**, Zakharova (Galanzha) EI. Modification of lymphoconstriction action of staphylococcal toxin by laser radiation. *Laser Tech Optoelectronics* 1992; **1-2**: 36-39
167 **Harshman S**, Boquet P, Duflot E, Alouf JE, Montecucco C, Papini E. Staphylococcal alpha-toxin: a study of membrane penetration and pore formation. *J Biol Chem* 1989; **264**: 14978-14984
168 **Ward RJ**, Leonard K. The Staphylococcus aureus alpha-toxin channel complex and the effect of Ca^{2+} ions on its interaction with lipid layers. *J Struct Biol* 1992; **109**: 129-141
169 **Browse NL**, Stewart G. Lymphoedema: pathophysiology and classification. *J Cardiovasc Surg* (Torino) 1985; **26**: 91-106
170 **The diagnosis and treatment of peripheral lymphedema**. Consensus document of the International Society of Lymphology. *Lymphology* 2003; **36**: 84-91
171 **Bruns F**, Schueller P. Novel Treatment Options in Secondary Lymphedema. *AAHPM Bulletin* 2005; 5-7
172 **Szuba A**, Rockson SG. Lymphedema: anatomy, physiology and pathogenesis. *Vasc Med* 1997; **2**: 321-326
173 **Witte CL**, Witte MH, Unger EC, Williams WH, Bernas MJ, McNeill GC, Stazzone AM. Advances in imaging of lymph flow disorders. *Radiographics* 2000; **20**: 1697-1719
174 **Földi E**, Földi M, Clodius L. The lymphedema chaos: a lancet. *Ann Plast Surg* 1989; **22**: 505-515
175 **Gregl A**. [Secondary leg edema--experimental study]. *Z Lymphol* 1988; **12**: 48-53
176 **Pflug JJ**, Calnan JS. The experimental production of chronic lymphoedema. *Br J Plast Surg* 1971; **24**: 1-9
177 **Kinjo O**, Kusaba A. Lymphatic vessel-to-isolated-vein anastomosis for secondary lymphedema in a canine model. *Surg Today* 1995; **25**: 633-639
178 **Galanzha EI**, Tuchin VV, Solov'eva AV, Stepanova TV, Brill GE and Zharov VP. Development imaging and experimental model for studying pathogenesis and treatment efficacy of postmastectomy lymphedema. *Proc SPIE* 2002; **4624**: 123-129
179 **Galanzha EI**, Solov'eva AV, Stepanova TV, Tuchin VV, Brill GE and Zharov VP. Analysis of lymph microcirculation in norm, at the experimental lymphedema and pathological stress on animal model. Abstracts of the 22nd Meeting of the European Society for Microcirculation. Exeter, Devon, United Kingdom. August 28-30, 2002. *J Vasc Res* 2002; **39** Suppl 1**:** 9-99
180 **Solov'eva AV**, Brill GE, Galanzha EI, Stepanova TV. Stress-induced changes in lymph microcirculation. *Proc SPIE* 2004; **4241**: 309-311
181 **Solov'eva AV**, Galanzha EI, Stepanova TV, Brill' GE. Changes in lymph microcirculation during pathological stress. *Bull Exp Biol Med* 2002; **134**: 241-243
182 **Tuchin VV**. Optical clearing of tissue and blood using the immersion method. *J Phys D: Appl Phys* 2005; **38**: 2497-2518
183 **Tuchin VV**. Optical immersion as a new tool for controlling the optical properties of tissues and blood. *Laser Physics* 2005; **15**: 1109-1136
184 **Columbano A**. Cell death: current difficulties in discriminating apoptosis from necrosis in the context of pathological processes in vivo. *J Cell Biochem* 1995; **58**: 181-190
185 **Brauer M**. In vivo monitoring of apoptosis. *Prog Neuropsychopharmacol Biol Psychiatry* 2003; **27**: 323-331
186 **Darzynkiewicz Z**, Bedner E, Traganos F. Difficulties and pitfalls in analysis of apoptosis. *Methods Cell Biol* 2001; **63**: 527-546
187 **Alenzi FQ**, Wyse RK, Altamimi WG. Apoptosis as a tool for therapeutic agents in haematological diseases. *Expert Opin Biol Ther* 2004; **4**: 407-420
188 **Haas RL**, de Jong D, Valdés Olmos RA, Hoefnagel CA, van den Heuvel I, Zerp SF, Bartelink H, Verheij M. In vivo imaging of radiation-induced apoptosis in follicular lymphoma patients. *Int J Radiat Oncol Biol Phys* 2004; **59**: 782-787
189 **Yan SD**, Stern DM. Mitochondrial dysfunction and Alzheimer's disease: role of amyloid-beta peptide alcohol dehydrogenase (ABAD). *Int J Exp Pathol* 2005; **86**: 161-171
190 **Gradl G**, Gaida S, Gierer P, Mittlmeier T, Vollmar B. In vivo evidence for apoptosis, but not inflammation in the hindlimb muscle of neuropathic rats. *Pain* 2004; **112**: 121-130
191 **Al-Gubory KH**. Fibered confocal fluorescence microscopy for imaging apoptotic DNA fragmentation at the single-cell level in vivo. *Exp Cell Res* 2005; **310**: 474-481
192 **Chan K**, Truong D, Shangari N, O'Brien PJ. Drug-induced mitochondrial toxicity. *Expert Opin Drug Metab Toxicol* 2005; **1**: 655-669
193 **Alenzi FQ**. Apoptosis and diseases: regulation and clinical relevance. *Saudi Med J* 2005; **26**: 1679-1690
194 **Hunter AL**, Choy JC, Granville DJ. Detection of apoptosis in cardiovascular diseases. *Methods Mol Med* 2005; **112**: 277-289
195 **Nagata S**. Apoptosis and autoimmune diseases. *IUBMB Life* 2006; **58**: 358-362
196 **Desmettre T**, Devoisselle JM, Mordon S. Fluorescence properties and metabolic features of indocyanine green (ICG) as related to angiography. *Surv Ophthalmol* 2000; **45**: 15-27
197 **Bollinger A**, Saesseli B, Hoffmann U, Franzeck UK. Intravital detection of skin capillary aneurysms by videomicroscopy with indocyanine green in patients with progressive systemic sclerosis and related disorders. *Circulation* 1991; **83**: 546-551

198 **Borotto E**, Englender J, Pourny JC, Naveau S, Chaput JC, Lecarpentier Y. Detection of the fluorescence of GI vessels in rats using a CCD camera or a near-infrared video endoscope. *Gastrointest Endosc* 1999; **50**: 684-688

199 **Wei X**, Runnels JM, Lin CP. Selective uptake of indocyanine green by reticulocytes in circulation. *Invest Ophthalmol Vis Sci* 2003; **44**: 4489-4496

200 **Kitai T**, Inomoto T, Miwa M, Shikayama T. Fluorescence navigation with indocyanine green for detecting sentinel lymph nodes in breast cancer. *Breast Cancer* 2005; **12**: 211-215

201 **Moneta G**, Brülisauer M, Jäger K, Bollinger A. Infrared fluorescence videomicroscopy of skin capillaries with indocyanine green. *Int J Microcirc Clin Exp* 1987; **6**: 25-34

S- Editor Liu Y **L- Editor** Lutze M **E- Editor** Bai SH